Numerical modelling of meteorological tsunamis in the southern Strait of Georgia, with application to Boundary Bay

Alexander Rabinovich, Jadranka Šepić, Richard Thomson and Nicky Hastings

Fisheries and Oceans Canada
Institute of Ocean Sciences
9860 West Saanich Road
Sidney, BC V8L 4B2, CANADA

2023

Canadian Technical Report of Hydrography and Ocean Sciences 369

Fisheries and Oceans Canada | Pêches et Océans Canada

Canada

Canadian Technical Report of Hydrography and Ocean Sciences

Technical reports contain scientific and technical information of a type that represents a contribution to existing knowledge, but which is not normally found in the primary literature. The subject matter is generally related to programs and interests of the Oceans and Science sectors of Fisheries and Oceans Canada.

Technical reports may be cited as full publications. The correct citation appears above the abstract of each report. Each report is abstracted in the data base Aquatic Sciences and Fisheries Abstracts.

Technical reports are produced regionally but are numbered nationally. Requests for individual reports will be filled by the issuing establishment listed on the front cover and title page.

Regional and headquarters establishments of Ocean Science and Surveys ceased publication of their various report series as of December 1981. A complete listing of these publications and the last number issued under each title are published in the Canadian Journal of Fisheries and Aquatic Sciences, Volume 38: Index to Publications 1981. The current series began with Report Number 1 in January 1982.

Rapport technique canadien sur l'hydrographie et les sciences océaniques

Les rapports techniques contiennent des renseignements scientifiques et techniques qui constituent une contribution aux connaissances actuelles mais que l'on ne trouve pas normalement dans les revues scientifiques. Le sujet est généralement rattaché aux programmes et intérêts des secteurs des Océans et des Sciences de Pêches et Océans Canada.

Les rapports techniques peuvent être cités comme des publications à part entière. Le titre exact figure au-dessus du résumé de chaque rapport. Les rapports techniques sont résumés dans la base de données Résumés des sciences aquatiques et halieutiques.

Les rapports techniques sont produits à l'échelon régional, mais numérotés à l'échelon national. Les demandes de rapports seront satisfaites par l'établissement auteur dont le nom figure sur la couverture et la page de titre.

Les établissements de l’ancien secteur des Sciences et Levés océaniques dans les régions et à l'administration centrale ont cessé de publier leurs diverses séries de rapports en décembre 1981. Vous trouverez dans l'index des publications du volume 38 du Journal canadien des sciences halieutiques et aquatiques, la liste de ces publications ainsi que le dernier numéro paru dans chaque catégorie. La nouvelle série a commencé avec la publication du rapport numéro 1 en janvier 1982.

Canadian Technical Report of
Hydrography and Ocean Sciences 369

2023

NUMERICAL MODELLING OF METEOROLOGICAL TSUNAMIS IN THE SOUTHERN STRAIT OF GEORGIA, WITH APPLICATION TO BOUNDARY BAY

Alexander Rabinovich[1], Jadranka Šepić[2], Richard Thomson[1], and Nicky Hastings[3]

[1]Fisheries and Oceans Canada
Institute of Ocean Sciences
9860 West Saanich Road
Sidney, BC V8L 4B2, CANADA

[2]Faculty of Science
University of Split
33 Ruđera Boškovića
Split, 21000, CROATIA

[3]Natural Resources Canada
Geological Survey of Canada - Pacific Division
605 Robson Street
Vancouver, BC V6B 5J3, CANADA

Cat. No. Fs97-18/369E-PDF ISBN 978-0-660-68789-6 ISSN 1488-5417

Correct citation for this publication:

Rabinovich, A., Šepić, J., Thomson, R., and Hastings, N., 2023. Numerical modelling of meteorological tsunamis in the southern Strait of Georgia, with application to Boundary Bay. Can. Tech. Rep. Hydrogr. Ocean Sci. 369: v + 49 p.

CONTENTS

ABSTRACT

Rabinovich, A., Šepić, J., Thomson, R., and Hastings, N., 2023. Numerical modelling of meteorological tsunamis in the southern Strait of Georgia, with application to Boundary Bay. Can. Tech. Rep. Hydrogr. Ocean Sci. 369: v + 49 p.

Meteorological tsunamis are tsunami-like waves generated by atmospheric processes. A number of meteotsunamis have been recorded recently for the coast of British Columbia, including the southern Strait of Georgia. A previous statistical analysis of tide gauge records found that meteotsunamis are frequent occurrences in the region and that they are strongly affected by local topographic features.

As no sea level data were available for Boundary Bay, we determined the meteotsunami risk for the region using a high-resolution numerical model. The measured speeds and directions of atmospheric disturbances that propagated over the southern Strait of Georgia during the major meteotsunami of 1 November 2010 were used to force the model for subsequent verification against tide gauge records. The numerical experiments revealed strongly individual sea level responses at each gauged site to air pressure disturbance properties. Differences in the local topography and coastline geometry were found to be responsible for the variations in response among sites.

Following verification, the model was used to simulate meteotsunamis for the Boundary Bay region. The maximum simulated wave amplitudes increase from 5-6.5 cm in the open ocean to 51 cm at the entrance to the bay. Meteotsunami-generated currents for the region attain maximum speeds of only 11.5 cm/s. For optimal disturbance propagation speeds of between 15 and 35 m/s, the computed currents were up to 25 cm/s for the areas of the Tsawwassen Ferry Terminal and east mainland coast. However, within the inner sector of Boundary Bay, sea level oscillations and currents were less than 4 cm and 4 cm/s, respectively. We conclude that the bathymetry of Boundary Bay helps shelter it from significant meteotsunamis originating in the southern Strait of Georgia.

RÉSUMÉ

Rabinovich, A., Šepić, J., Thomson, R., and Hastings, N., 2023. Numerical modelling of meteorological tsunamis in the southern Strait of Georgia, with application to Boundary Bay. Can. Tech. Rep. Hydrogr. Ocean Sci. 369: v + 49 p.

Les tsunamis météorologiques sont des vagues de type tsunami générées par des processus atmosphériques. Un certain nombre de météotsunamis ont été enregistrés récemment sur la côte de la Colombie-Britannique, y compris dans le sud du détroit de Géorgie. Une analyse statistique précédente des enregistrements des marégraphes a révélé que les météotsunamis sont des phénomènes fréquents dans la région et qu'ils sont fortement affectés par les caractéristiques topographiques locales.

Comme aucune donnée sur le niveau de la mer n'était disponible pour Boundary Bay, nous avons déterminé le risque de météotsunami pour la région à l'aide d'un modèle numérique à haute résolution. Les vitesses et directions mesurées des perturbations atmosphériques qui se sont propagées dans le sud du détroit de Géorgie lors du météotsunami majeur du 1er novembre 2010 ont été utilisées pour forcer le modèle à être vérifié ultérieurement par rapport aux enregistrements des marégraphes. Les expériences numériques ont révélé des réponses fortement individuelles du niveau de la mer sur chaque site jaugé aux propriétés de perturbation de la pression atmosphérique. Il a été constaté que les différences dans la topographie locale et la géométrie du littoral étaient responsables des variations de réponse entre les sites.

Après vérification, le modèle a été utilisé pour simuler des météotsunamis pour la région de Boundary Bay. Les amplitudes maximales des vagues simulées augmentent de 5 à 6,5 cm en haute mer à 51 cm à l'entrée de la baie. Les courants générés par les météotsunamis dans la région atteignent des vitesses maximales de seulement 11,5 cm/s. Pour des vitesses optimales de propagation des perturbations comprises entre 15 et 35 m/s, les courants calculés atteignaient 25 cm/s pour les zones du terminal ferry de Tsawwassen et de la côte est du continent. Cependant, dans le secteur intérieur de Boundary Bay, les oscillations du niveau de la mer et les courants étaient respectivement inférieurs à 4 cm et 4 cm/s. Nous concluons que la bathymétrie de Boundary Bay contribue à la protéger des météotsunamis importants provenant du sud du détroit de Géorgie.

Looking southeastward from Boundary Bay toward Mt. Baker

1. INTRODUCTION

"*Meteorological tsunamis*" ("*meteotsunamis*") are long destructive oceanic waves that have the same temporal and spatial scales as ordinary tsunami waves and can affect coastal areas in a similar hazardous way, but which are generated by atmospheric forcing (atmospheric gravity waves, pressure jumps, frontal passages, squall lines, etc.) rather than by seismic activity or submarine landslides [*Rabinovich and Monserrat*, 1996; *Monserrat et al.*, 2006]. Meteotsunamis have long been considered a very rare and local phenomenon that occurs only in a few specific harbours, such as Ciutadella (Balearic Islands, Spain), Vela Luka and Stari Grad (Croatia), Mazaro dell Vallo (Sicily), Nagasaki Bay (Japan) and the Great Lakes [*Ewing et al.*, 1954; *Monserrat et al.*, 2006; *Rabinovich,* 2009]. However, observations from around the world over the past decade and occurrences of several devastating events, including the 2017-2018 meteotsunamis in the Netherlands, Republic of South Africa, Brazil and Florida (USA), have demonstrated that meteotsunamis are much more common and widespread than was previously thought [*Pattiaratchi*

and Wijeratne, 2015; *Rabinovich*, 2020]. The tragic event in the Persian Gulf of 19 March 2017, when 5 people were killed on the coast of Dayyer, Iran [*Salaree et al.*, 2018; *Heidarzadeh et al.*, 2020], once again showed the severe threat of this phenomenon for coastal areas, even for the regions where meteotsunamis had never been reported before. Data analysis and numerical experiments have shown that meteotsunamis are commonly a *resonant* phenomenon governed by the Froude number, *Fr*, which is the ratio of the atmospheric gravity wave speed (U) to the phase speed of long ocean waves (c); resonance occurs when $Fr = U/c \sim 1.0$ [cf. *Šepić et al.*, 2015].

In some regions of the world (cf. Spain, Croatia, Italy, Japan, Australia and the Great Lakes) meteorological tsunamis occur rather regularly, while in some others, including the coast of British Columbia (BC), they are relatively rare and not so well known. The first meteotsunami in BC was identified on 9 December 2005, when the event was sufficiently strong to trigger an automatic tsunami alarm [*Stephenson and Rabinovich*, 2009; *Thomson et al.*, 2009]. Since then, the network of digital tide gauges and atmospheric pressure sensors have enabled researchers to identify several meteotsunami events along the BC coast. The high meteotsunami risk for some exceptional locations is mainly related to a combination of shelf topography and coastline geometry, which together create favourable resonant wave conditions. The shallow Boundary Bay area of the southern Strait of Georgia is of particular interest because of the possibility of hazardous seas level responses to the marked atmospheric disturbances that frequently transit the region [cf. *Thomson et al.*, 2009].

During the late 1990s, the Canadian Hydrographic Service (CHS) and the National Oceanic and Atmospheric Administration (NOAA) upgraded their sea level networks with digital high precision tide gauges having a 1-min sampling interval. Moreover, a school meteorological network of 132 high precision meteorological stations (www.victoriaweather.ca) is now available for the area of Vancouver Island [*Weaver and Wiebe*, 2006]. This network enables us to examine the physics of meteotsunami-generating air pressure disturbances, including very precise estimation of the disturbance velocities, dispersion and spatial structure. Observed air pressure disturbances can be used as input into numerical models so that the sea level response at different locations can be estimated more precisely.

Rabinovich et al. [2019] focuses on non-seismic tsunami-like waves (meteotsunamis) in the Boundary Bay region of the southern Strait of Georgia. The study uses an 11-year dataset of 1-min

records from three nearest tide gauges - Point Atkinson (CHS), Cherry Point and Friday Harbor (both NOAA stations) – to examine sea level oscillations generated by high-frequency air pressure disturbances, which are a common occurrence in this region. The events were found to have a marked seasonal periodicity, with wave variance (energy) in winter roughly twice that of summer. However, extreme meteotsunami events potentially can occur at any time of year. Based on the statistical analysis of tide gauge records for the 11-year period 2008-2018, *Rabinovich et al.* [2019] found that major events (>10 cm) were most often observed at Cherry Point (124 times) and were much rarer at Friday Harbor (32 times) and Point Atkinson (7 times). The maximum recorded wave heights at these stations were 16.7 cm, 17.2 cm and 13.1 cm, respectively. Although none of the events appear to have affected Boundary Bay, additional data inside the bay and high-resolution numerical modelling are required for reliable determination of the meteotsunami risk for the region.

It should be emphasized that even relatively weak meteotsunamis can produce significant, even destructive, currents. In particular, a tragic event occurred near Warren Dunes, a beach along the southeast shoreline of Lake Michigan on 4 July 2003, when a moderate-height (~0.3 m) meteotsunami generated strong off-shore currents that drowned seven people [*Linares et al.*, 2019]. Another example is a medium-size meteotsunami (a few tens of centimeters wave height) that affected Mali Ston Bay sandwiched between the mainland and the Pelješac Peninsula (Croatia) on 27 June 2003. The swift currents associated with this event caused major damage to shellfish farms in the bay [*Vilibić et al.*, 2004].

Intense currents associated with meteotsunamis have also been observed in the Strait of Georgia. In particular, on 13 July 2007 a local residents Ken Youds of Thetis Island sent the following eye-witness report: "…*At about 5 a.m. I could see the inlet water flowing in (as if it was an incoming tide) at an unusually fast rate… I then noticed that the dock was being forcibly shifted southward by the unusually strong inflowing tide -- as though it was a 2-3 knot current. I have done a lot of kayaking along the BC coast, including through tidal currents, so am familiar with gauging current speed. …As I was staring at the fast moving water, I noticed it start to swirl. Kelp, buoys, lines of the dock all started to twist about, and then the water began to move rapidly (2-3 knots) outwards (toward the north, where in inlet entrance is). I watched for about a minute, and then the tidal surge reversed again, running inward. After another minute or so, it reversed again. I kept watching and wishing I could share this event with someone, but alas everyone was sound*

asleep. I knew that I was watching the inlet (which is 100 meters across) behave as if it was a surge channel, and therefore I concluded that some kind of physical event had happened somewhere to cause this." [*Thomson et al.*, 2009].

Similarly, on 1 November 2010, an unusual marine event was observed by several local people near Point Atkinson in the southern Strait of Georgia. One person, Gil Floyd, sent the following e-mail to the Canadian Hydrographic Service (CHS): *"Location: Eagle Harbour & Fisherman's Cove. Prior to 09:00* <PST> *on November 01, 2010 the channel water was relatively clear. Then at 09:00 a wall of very muddy water about 2 inches high surged into the channel running North to south. This fast moving out flow tide lasted for less than 1/2 hour. Then surged back the opposite way south to north, incoming. By 10:00 it was running very fast North to South again. When I pulled my prawn traps yesterday the first 200 feet of sea was clean. The bottom 100 ft was very muddy… The strength of the tide was something like you would see on the east coast. Wall of muddy water dissipated by late morning…".* The following examination of the event, including processing of several tide gauge and numerous air pressure records, indicated that this was a meteotsunami generated by atmospheric disturbances propagating westward with a speed of 20-25 m/s [*Rabinovich et al.*, 2020].

From these two examples, it is evident that meteorological tsunamis impact the southern Strait of Georgia and that their properties need to be examined in detail. Multiple observations of meteotsunamis around the world have shown that the effectiveness of their generation strongly depends on specific parameters of propagating atmospheric disturbances. The catastrophic events are normally associated with exclusive "*resonant*" combination of these parameters, which further depend on the geometry of the coastline and bathymetry of the adjacent region. The best way to identify these parameters is through numerical experiments [cf. *Orlić et al.*, 2010; *Šepić et al.*, 2018; *Rabinovich et al.*, 2021, 2023].

2. NUMERICAL MODELLING OF METEOTSUNAMIS: AN OVERVIEW

In the past two decades, there has been considerable progress in the numerical modelling of seismically-generated tsunamis. Modern tsunami models allow us to gain insight into the physics of tsunami generation and to accurately reproduce actual tsunami waves [cf. *Titov and González*, 1997; *Titov and Synolakis*, 1998; *Kowalik et al.*, 2007; *Fine et al.*, 2015]. Major tsunamis, such as

the 2004 Sumatra tsunami, recorded some 15,000-20,000 km from the source area, are reconstructed by global numerical tsunami models with remarkably high precision [*Titov et al.*, 2005; *Rabinovich et al.*, 2011, 2017]. Tsunami models began to be one of the effective tools of tsunami investigation. These models are widely used for various problems, in particular for [cf. *Fujii and Satake*, 2007; *Titov et al.*, 2016]:

(1) Real-time tsunami modelling and warning.

(2) Reconstruction of actual events and comparison with observations.

(3) Reconstruction of the tsunami source.

(4) Long-term tsunami forecasts and estimation of the tsunami risk for specific coastal regions.

Compared to seismically-generated tsunamis, there have been relatively few numerical modelling studies of meteotsunamis. Moreover, for meteotsunamis, only targets (2) and (4) are presently realistic. Numerical modelling of meteotsunamis enable us to better understand the physics and nature of this phenomenon, to define the generation mechanisms and transformations of events and to estimate maximum expected meteotsunami wave heights for specific regions.

One of the first attempts to use numerical modelling to examine properties of meteotsunamis in a particular region was undertaken by *Rabinovich et al.* [1999]. In their study, the authors simulated waves in Ciutadella Inlet (Figure 1), known as one of the "hottest" meteotsunami sites [cf. *Rabinovich and Monserrat*, 1996], where meteotsunamis, locally known as *rissaga*, occur more often and have higher amplitudes than in any <other known> place in the world. The two main targets of the study were:

(1) To estimate the resonant periods of the eigen modes of Ciutadella Inlet and adjacent Platja Grant Inlet (Figure 1a).

(2) To estimate the amplification of incoming waves in these inlets as functions of the incident angle.

As this study was intended to model the response to free waves generated at the open boundary, we did not consider atmospheric waves as possible forcing (input). Two types of input function were applied at the boundary: (a) a half-wave with a fixed period; and (b) random noise with a high-frequency component expressed by a first order autoregressive (AR) model.

The *numerically computed* periods of the fundamental (Helmholtz) mode, together with the first and second eigen modes, were respectively 11.1, 4.7 and 2.35 min for Ciutadella Inlet, while

the corresponding *observed* periods from the LAST-97 experiment (July-September 1997) were 10.6, 4.4 and 2.45 min [*Monserrat et al.*, 1998]. The computed (and observed) periods for Platja Gran were 6.1 (5.5), 3.6(xx[1]) and 2.4 (2.2) min. What is also important is that the results of numerical modelling allowed the authors to estimate the wave amplification between the middle of the inlet (point Y4, which was selected to be close to the position of the local tide gauge CS, that was working during the period of 1989-90, see *Rabinovich and Monserrat* [1996]) and the head of the inlet (point Y5; see locations of Y4 and Y5 in Figures 1a and 1c). The corresponding amplification factor was 1.23. This means, for example, that the wave of 196.7 cm recorded on 6 July 1989 at CS in Ciutadella Inlet was approximately 240 cm at the head of the inlet.

Another principal result of the *Rabinovich et al.* [1999] study is an estimation of the incident angle influence on the relative amplification of waves in Ciutadella Inlet. The computations were done for different angles of incidence (φ) of the input semi-wave using three values of the initial period, T_0: 5, 10 and 20 min. It is evident (Figure 1d) that the maximum amplification is reached when the wave propagates from the southwest (190°-250°). The extreme amplification is achieved when $\varphi = 220°$, which correlated well with the direction of atmospheric waves producing *rissaga* in Ciutadella [*Monserrat and Thorpe*, 1992].

Two factors appear to determine this specific direction:

(1) This direction approximately coincides with the orientation of Ciutadella Inlet (Figure 1a).

(2) It also coincides with the orientation of the southeast shelf of Mallorca Island (Figure 1b): in effect, the wave propagating along the SE shelf of Mallorca is "aiming" directly at Ciutadella Inlet.

The combination of these two factors explains why this particular direction, 220° True, is effective; atmospheric waves propagating in this direction generate ocean waves on the SE shelf of Mallorca that enter straight into Ciutadella Inlet. In contrast, when the initial wave propagates along the southwest shelf of Menorca Island (~130° or 310° True), the amplification is minimal. Atmospheric waves arriving from the opposite (NE) side of Menorca Island generate no seiches (rissaga waves) in Ciutadella Inlet.

[1] The exact observed period of the first mode in Platja Gran was undetectable because the instrument was located very close to theoretical location of the nodal line for that mode.

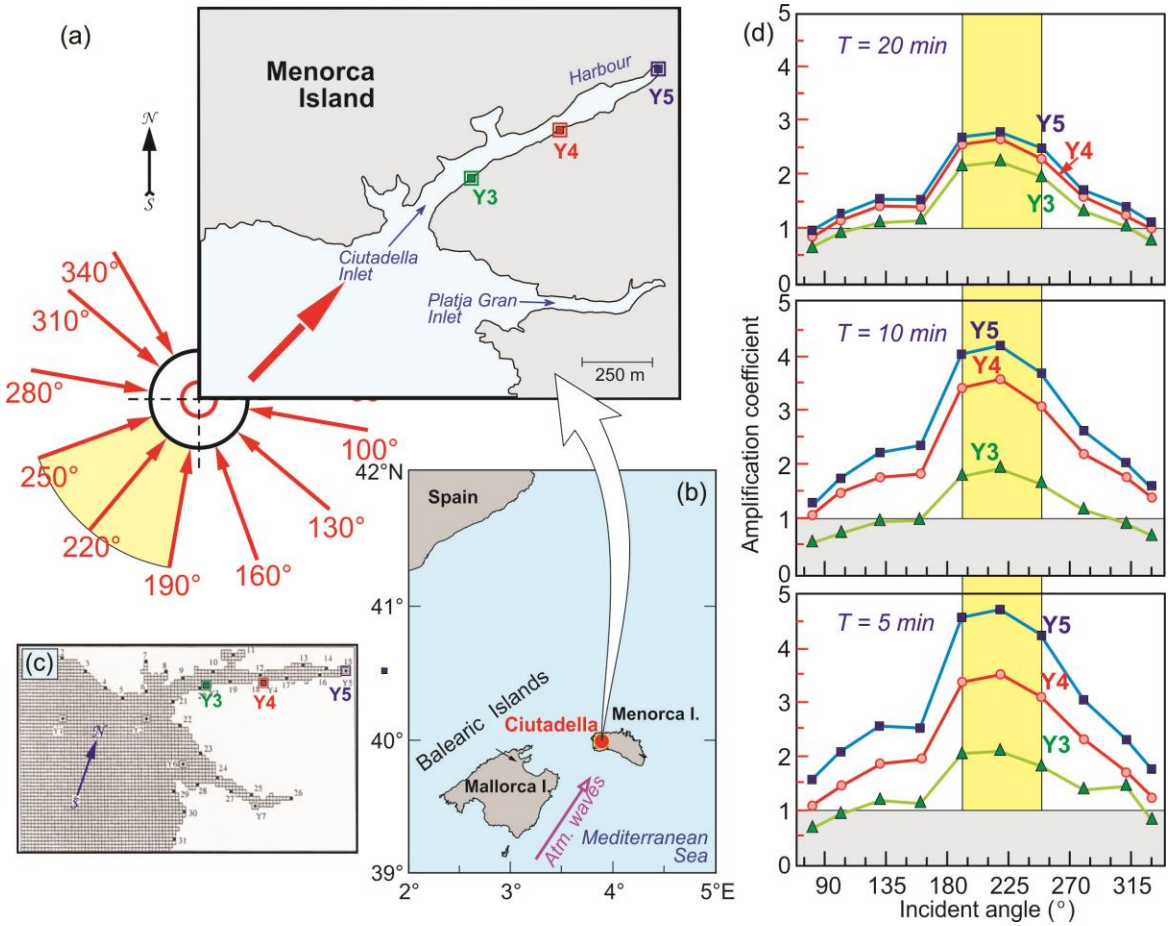

Figure 1. Numerically computed amplification of the incoming wave in Ciutadella Inlet, Menorca Island, Spain. (a) Map of Ciutadella and Platja Gran inlets on the western coast of Menorca Island. The red thin arrows indicate wave directions used in the numerical experiments, the yellow sector border denotes the most effective wave directions, and the thick red arrow shows the direction of 220° True for maximum wave amplification; (b) Map of the Balearic Islands (Spain) showing the location of Ciutadella on the west coast of Menorca Island; the purple arrow indicates the atmospheric waves generating meteotsunamis (locally known as *rissaga*) in Ciutadella Inlet; (c) The computational domain used in numerical experiments; Y3, Y4 and Y5 are three selected computational points in Ciutadella Inlet; and (d) Amplification of incoming waves with initial semi-periods of 5, 10 and 20 min in Ciutadella Inlet (at points Y3, Y4 and Y5) as a function of the incident angle (modified from *Rabinovich et al.* [1999]).

The numerical experiments of *Rabinovich et al.* [1999] demonstrate the role of the atmospheric wave directions in the formation of meteotsunamis. Basically, there are "favourable" and "unfavourable" directions. At the same time, the sector of "favourable" directions is relatively

wide so, for example, the differences in computed amplification coefficients for directions of 190°, 220° and 250° are small (Figure 1d). The crucial factor influencing the generation of meteotsunamis is the speed, U, of the atmospheric disturbance and its closeness to the speed of the generated ocean waves, $c = \sqrt{gh}$, where g is the gravity acceleration, $h = h(x, y)$ is the water depth and x, y are the horizontal Cartesian coordinates. The maximum amplification occurs for the critical speed, $U = c$, corresponding to the speed for *Proudman resonance* [*Proudman*, 1929]. For the study region, the principal areas where such resonance can be expected are the SE shelf of Mallorca Island and the SW shelf of Menorca Island. We assume that in producing destructive meteotsunamis like those in 1984 and 2006, the Proudman resonance played a determining role. In *Rabinovich et al.* [1999], this factor was not examined; however, in the following studies on numerical modelling of meteotsunamis, this factor was of primary concern.

Additional numerical modelling of the Menorca Island region (Figure 1a) was conducted by *Liu et al.* [2003]. A uniform grid with spatial resolutions $\Delta x = \Delta y = 10$ m was used, resulting in 119×199 grid points. The sea level data measured at open sea Station MW4 from the LAST-97 experiment was used as the input function. The main purpose of the experiments was to examine the resonant coupling between two adjacent inlets, Ciutadella and Platja Gran. The eigen periods for both inlets were also computed and shown to be in good agreement with observations and with those computed by *Rabinovich et al.* [1999].

Vilibić et al. published a series of modeling studies [2004, 2008, 2010] that examined several major meteotsunami events. On 27 June 2003, a meteotsunami on the west coast of Croatia (known locally as a "*šćiga*") affected Stari Grad Bay (Hvar Island) and Mali Ston Bay (near the isthmus of the Pelješac Peninsula). The meteotsunami resulted in significant damage at these two sites. *Vilibić et al.* [2004] numerically simulated the event using a grid of 139×68 cells with a spatial resolution of 1 km and nested grids for the two bays with 50-m resolution. The model was forced by an air pressure disturbance estimated from a single station to have moved with a constant speed $U = 22$ m/s and direction $\varphi = 288°$ True. There were no sea level measurements in the two bays to verify the model, however, the model reasonably reproduced the observed low-frequency oscillations at several other sites. The results of the numerical modelling showed that the ocean wave formed in the Adriatic by a propagating air disturbance was resonantly amplified over the Adriatic shelf at depths of ~50 m due to the Proudman resonance. The resulting forced wave was

further amplified when it entered the funnel-shaped bays. The final significant amplification of this wave in the affected bays was due to harbour resonance.

Vilibić et al. [2008] investigated the destructive event of 15 June 2006 in Ciutadella Harbour (see Figure 1a for the location), when 5-m oscillations sank several dozen boats in the harbour and caused a total damage of over 30 million euros. Based on analysis of all available data, the authors estimated that the speed of the air pressure jump that had propagated over the region was U = 25 m/s with an incoming direction φ = 225°, which, according to *Rabinovich et al.* [1999], is the most favourable direction for generating strong seiches in Ciutadella Inlet (see Figure 1). The large-scale (coarse) model domain included the entire area of the Balearic Islands, with a grid resolution of 1' (i.e., 1.45 km × 0.92 km), and a computational domain of 241×121 grid cells. A nested grid with 10 m horizontal spatial resolution was used for Ciutadella Inlet and neighbouring Platja Gran Inlet; the incoming waves at the lateral boundaries were taken as the output of the coarse model. The simulation showed an abrupt sea level reaction to the propagating disturbance. Over the shelf, the oscillations were relatively small (a few centimeters) but as they approached the SW coast of Menorca they began to grow rapidly and reached 80 cm near the entrance to Ciutadella Inlet (Figure 1a). Due to harbour resonance of the incoming waves, the modelled sea levels amplified up to 230 cm. The inlet becomes shallow than the wave amplitude, producing a complete drying of the inner part of the harbour. These effects could not be completely reproduced by the model and this appears to be the main reason for some disagreement between the computed and observed wave heights.

Vilibić et al. [2010] used numerical modelling in an attempt to explain the 2-3 m tsunami-like waves observed on the Bulgarian coast of the Black Sea on 7 May 2007. The model domain encompassed the western Black Sea shelf, with a grid resolution of 30″ (i.e., 680 m × 925 m) The size of the computational domain was 259 × 299 grid cells. The model was forced by a moving air-pressure disturbance with a speed U = 16 m/s and direction (from) of φ = 210° True. The disturbance had a linear increase of air pressure of 3 hPa over 6 min. As shown in Figure 2, the numerical model reasonably well reproduced the observed properties of the sea level oscillations along the coast of Bulgaria and supported the assumption that the observed event was a meteotsunami. What is especially important is that the simulation results indicate certain "*hot spots*" (see *Šepić and Rabinovich* [2014] for definition), along the coast of maximum sea level

heights and current velocities. Because of the poor spatial resolution of the coastal geometry and bathymetry, we need to consider these results as preliminary, albeit remarkable if proven correct.

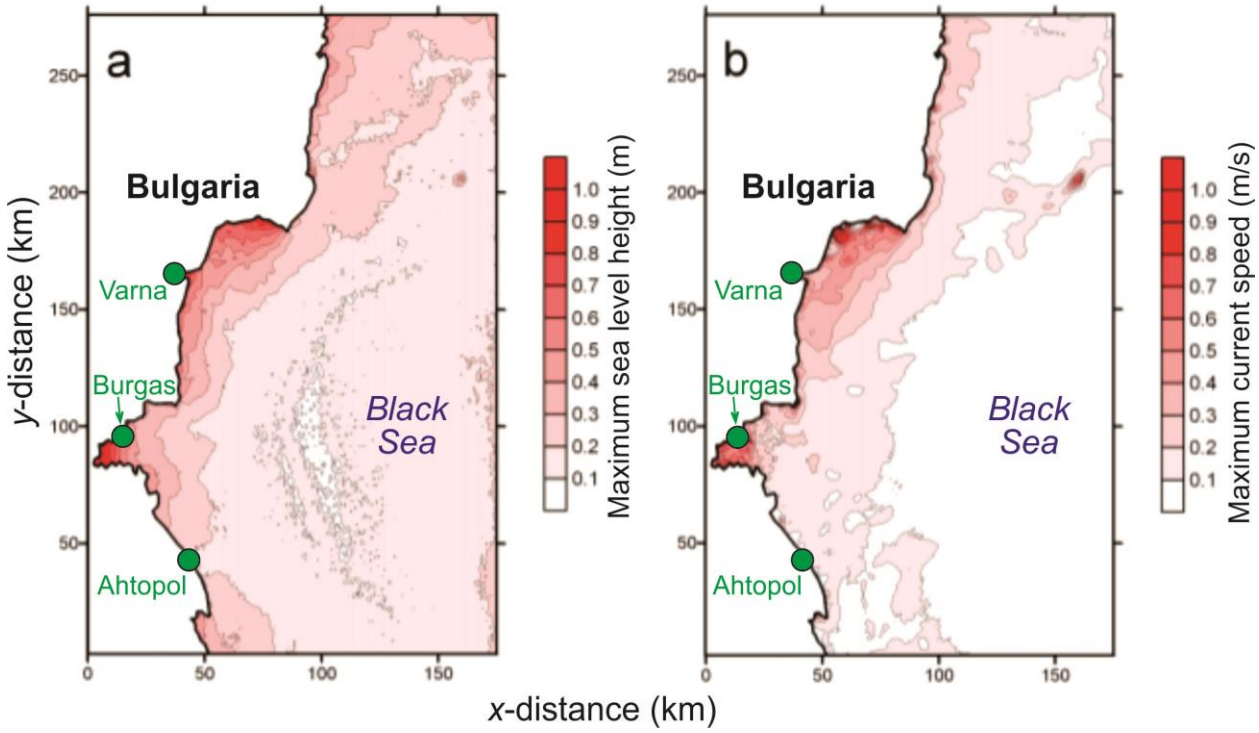

Figure 2. Results of meteotsunami simulation for the west coast of the Black Sea: (a) maximum sea level amplitudes and (b) maximum ocean currents (from *Vilibić et al.* [2010]).

An important numerical study of meteotsunamis was presented by *Orlić et al.* [2010]. The authors examined the catastrophic flood of 21 June 1978 in Vela Luka, Korčula Island, Croatia (Figures 3a,b). Tsunami-like waves having typical periods of about 20 min and trough-to-crest height up to 6 m heavily damaged the town and caused a state of emergency. The water flows exceeded 15 knots (7.5 m/s) as the waves sloshed back and forth along the harbour. This appears to be the largest reported meteotsunami in the 20th century. Pronounced sea level oscillations of ~ 1 m associated with the event were observed at a number of locations along both the east and west coasts of the Adriatic Sea.

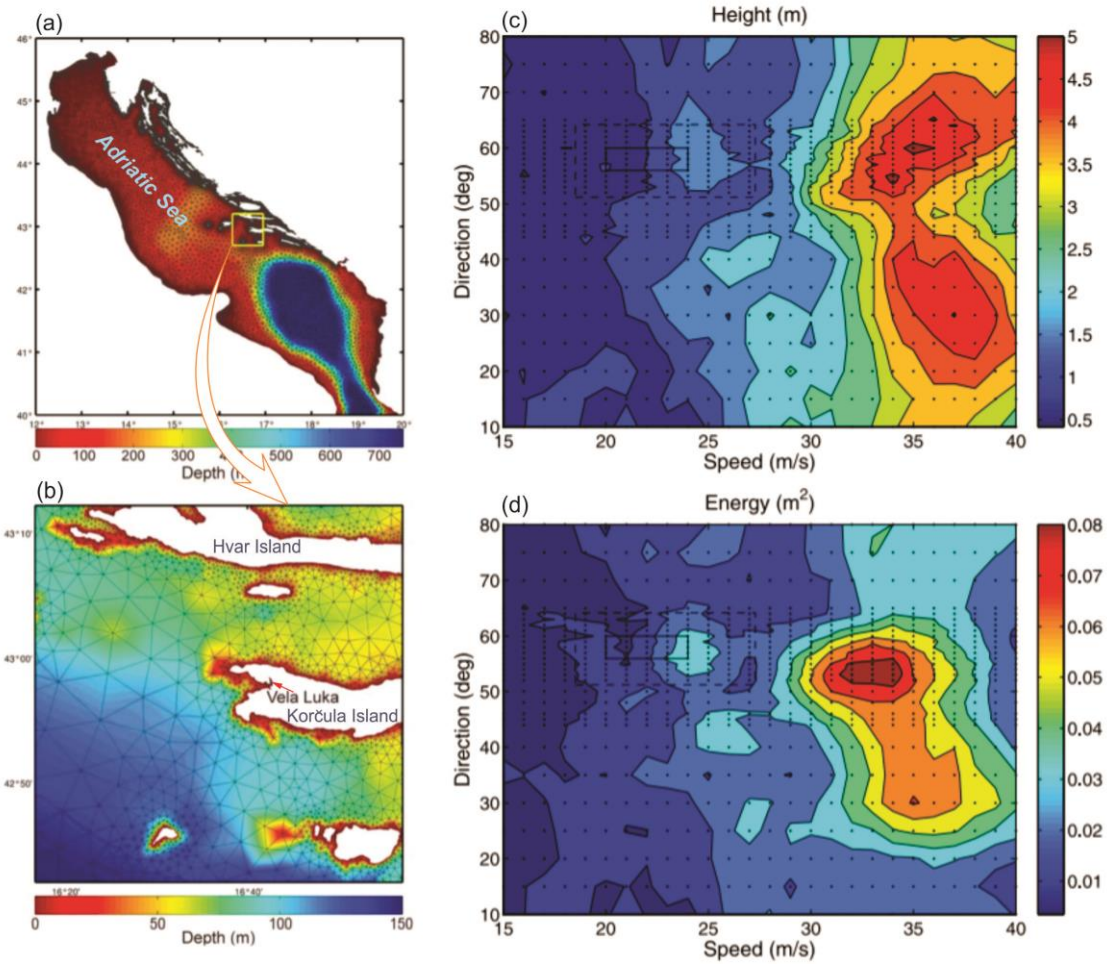

Figure 3. (a) The Adriatic Sea as resolved by the ADCIRC-2DDI finite element model; (b) a zoomed image of the Vela Luka area marked by the solid yellow rectangle in Figure 3b. The depth scales in Figures 3a and 3b are different; (c) difference between the maximum and minimum sea level amplitudes as functions of disturbance speed and direction (from); and (d) as for (c) but for the integral sea level energy obtained for the head of Vela Luka Bay by forcing the Adriatic model with a boxcar air pressure perturbation traveling at various speeds and directions. Each dot represents a run of the Adriatic model; the total number of runs was 754 (from *Orlić et al.* [2010]).

The authors applied a finite element (ADCIRC-2DDI) model; the numerical grid used for the computation included 44,965 elements and 26,956 nodes and so realistically represented the Adriatic Sea (Figure 3a). The finite element model (FEM) triangles were up to 7 km in the open Adriatic and as small as 150 m in Vela Luka Bay. The air pressure disturbance producing the sea level oscillations had the form of a boxcar function characterized by a 3 mbar increase in air

pressure that was 200 km wide and propagating across the Adriatic at varying speeds (U =15-40 m/s) and directions (ψ = 10-80°)[2]. As shown in Figures 3c,d, there are specific disturbance directions and speeds that most effectively generate strong oscillations in Vela Luka. The speed of the atmospheric disturbance is probably the most important parameter; the maximum oceanic waves are produced when the Proudman resonance takes place, i.e., when $U \sim c$, where c is the mean shallow-water wave speed between the Italian main coast and Vela Luka. This speed marginally depends on the atmospheric wave direction, ψ, whereby for ψ = 30°, the mean value of c = 32.6 m/s, and for ψ = 60°, c = 30.8 m/s. The closer c is to U, the stronger the amplification of the generated wave propagating from the coast of Italy to Vela Luka. As shown for Ciutadella Inlet [*Rabinovich et al.*, 1999], the direction of the atmospheric wave is not as critical as its propagation speed. For the relatively wide sector of disturbance propagation directions, ψ = 20-75°, the amplification of the wave in the harbour is approximately the same (Figure 3c).

In general, the numerical modeling experiments of *Orlić et al.* [2010] explain reasonably well the physical mechanism of the formation of the 1978 Vela Luka flood. Specifically, atmospheric waves moving across the Adriatic Sea at the speed $U \sim c$ resonantly generate intense sea level oscillations propagating towards Vela Luka Bay; these waves can further strongly amplify in Vela Luka Bay due to the funnelling effect of the bay and harbour resonance.

A similar finite element model was used by *Bechle and Wu* [2014] to explain two destructive meteotsunami events that occurred in Lake Michigan on 26 June 1954 and 6 July 1954. One of specific feature of these events was that both air pressure and wind perturbations were found essential to explain the observed floods.

Numerical experiments also helped *Šepić et al.* [2018] characterize the physical aspects of the "Odessa tsunami" that affected the beaches of Odessa and neighboring areas on 27 June 2014. The ensuing wave of 1-2 m injured six people and damaged beach structures. The authors used the General Bathymetric Chart of the Oceans (GEBCO) bathymetry (http://www.gebco.net/) with horizontal resolution of 30" (~650 m in longitude and 920 m in latitude). The model domain size was 650×451 grid points. Two alternative hypotheses, which were based on results of the data analysis, were examined: (1) sea level oscillations at Odessa were generated by a single air pressure disturbance propagating towards and over Odessa; and (2) these oscillations were generated by a

[2] Ψ is the direction TOWARD, while φ is the direction FROM ($\Psi=\varphi+180°$).

train of air pressure disturbances propagating along the northwestern shelf break. A number of numerical experiments were conducted to test both hypotheses. The model was forced by a bell-shaped air pressure disturbance given by:

$$\zeta_A = \frac{A}{1+(t/a)^{2\gamma}}, \quad (1)$$

where A = 3 hPa is the disturbance amplitude, a = 5 min is the half-width of the disturbance, and $\gamma = a/b$ is the slope parameter, where b = 100 seconds is the half-width of the increasing (decreasing) part of the pressure impulse. The disturbance was assumed to propagate over the domain with predefined speed and direction in two sets of experiments. The propagation parameters in both sets of experiments were chosen to vary in the following ranges: speed U = 5-35 m/s with an increment of 1 m/s, direction φ = 180-290º True at an increment of 5º.

Figure 4 shows the maximum predicted wave amplitudes as functions of speed and direction of the atmospheric disturbance for Experiment 1 (*direct forcing*). When a disturbance propagates directly over the Odessa site, the modelled waves reach their maximum amplitude of 52.7 cm (Figure 4a). This wave height corresponds to an air disturbance speed U = 14 m/s and direction φ = 180°. For this set of parameters, the maximum wave amplitudes for the entire domain are shown in Figure 4b. Simulated meteotsunami waves amplify northward along the propagation path. Water depths in this area range from 20 to 40 m, corresponding to a long wave phase speed c = 14.0-19.8 m/s. The Froude number, $Fr = U/c$ (the ratio of the disturbance speed to the longwave speed), ranges from 1.0 to 1.4, indicating favourable but not perfect conditions for Proudman resonance.

The authors also examined an alternative generation mechanism for the "Odessa tsunami". Maximum modelled wave amplitudes for Experiment 2 (*shelf break forcing*) are shown in Figure 5a as functions of the direction and speed of the atmospheric disturbance. There is a distinct point in the speed and direction distributions for which the sea level oscillations are most intense, specifically U = 27 m/s and φ = 230° True. For these specific parameters, the simulated waves on the Odessa coast have amplitudes of 28.3 cm (Figure 5b), while for the entire domain, modelled waves along the shelf break reach maximum heights of 50.0 cm. The waves undergo significant intensification while travelling along the shelf break, especially for depths of 70-80 m. It is over these depths that the long wave speed c = 26.2 - 28.0 m/s roughly matches the speed U = 27 m/s, of the air pressure disturbance so that Fr = 0.97-1.04 and Proudman resonance occurs. Because

the air pressure disturbance propagates over these depths for a considerable distance (~ 100 km), long ocean waves have enough time to accumulate the forcing energy and significantly intensify. Once the air pressure disturbance crosses over the shelf break into the deeper oceanic region, part of long sea waves reflects from the break, heading precisely toward the Odessa coast 200 km away along the western edge of a submarine canyon. Approaching the coast, waves further amplify due to the shoaling effect.

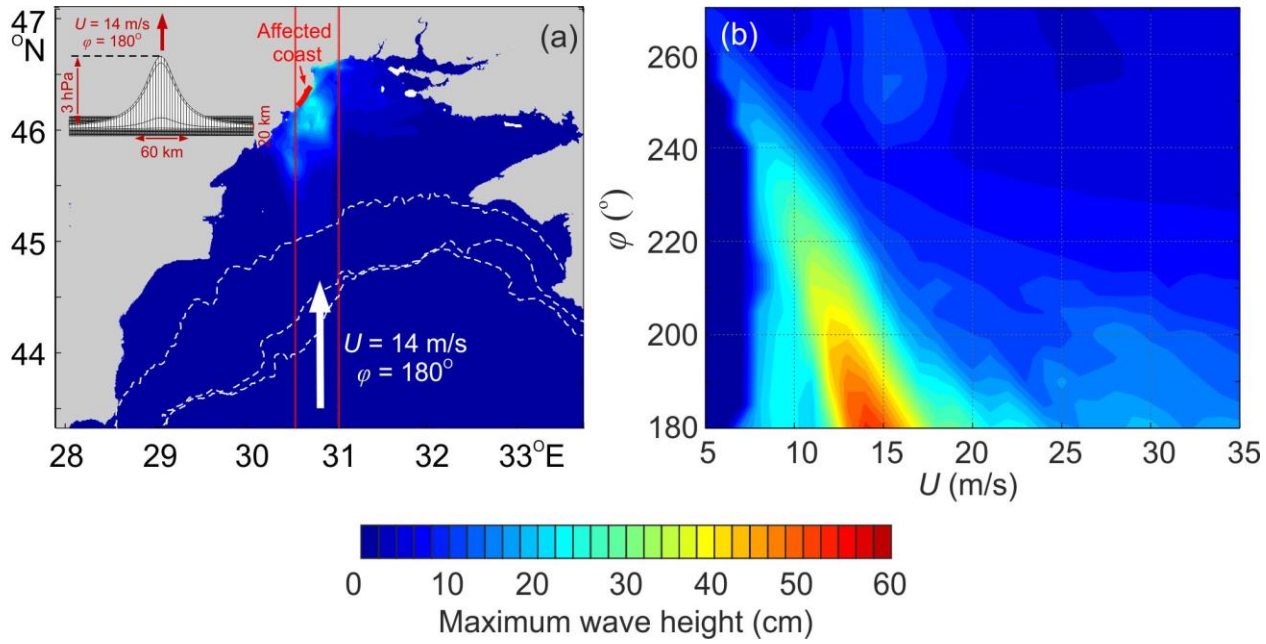

Figure 4. (a) Maximum simulated wave amplitudes within the Gulf of Odessa for the air pressure disturbance speed, U = 14 m/s, and direction, φ = 180° True; schematic of the air pressure disturbance is given in the upper left corner; (b) maximum simulated wave amplitudes at Odessa as a function of the disturbance speed, U, and direction, φ, of the propagating air pressure disturbance. Maximum amplitudes greater than 25 cm are restricted to the coastal points and are not easily distinguishable within the domain plot. Red lines in (a) border the propagation path of the air pressure disturbance; white dashed lines indicate depth contours of 50, 100 and 150 m. (From *Šepić et al.* [2018]).

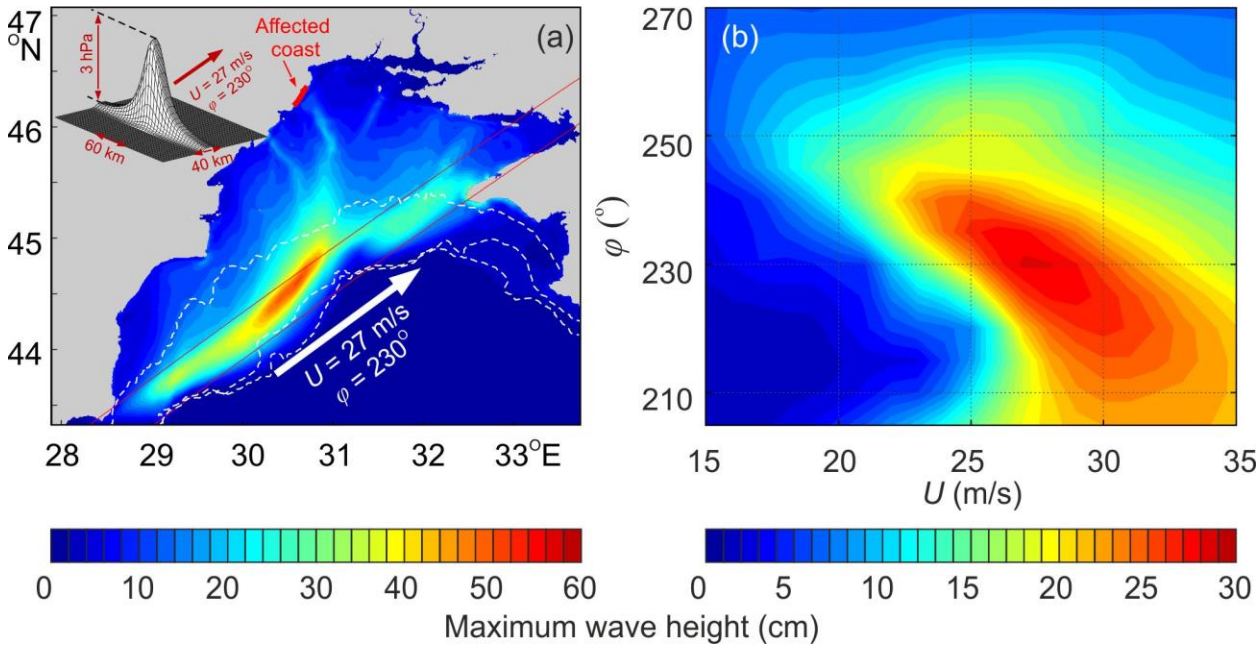

Figure 5. (a) Maximum modelled wave amplitudes within the model domain for an experiment in which an air pressure disturbance propagates with speed 27 m/s and direction (from) of 230° True; a schematic of the air pressure disturbance is given in the upper left corner; and (b) maximum simulated wave amplitudes at Odessa as functions of speed, U, and direction, φ, of the propagating air pressure disturbance. Maximum amplitudes greater than 25 cm are restricted to coastal sites and are not easily distinguishable over the domain plot. Red lines in (a) mark propagation paths of air pressure disturbances; white dashed lines indicate depth contours of 50, 100 and 150 m; and black line indicates the stretch of coast hit by meteotsunami waves. (From *Šepić et al*. [2018]).

The numerical studies considered above clearly demonstrated that:

(1) Modern numerical models of meteorological tsunamis can realistically reproduce the actual events. For further progress, two factors are crucial: (a) Better knowledge of the 2D structure of the atmospheric tsunamigenic disturbances and their temporal and spatial evolution; and (b) high-resolution bathymetric data for the study regions.

(2) The effectiveness of the meteotsunami generation mechanism is highly sensitive to the parameters of the propagating atmospheric disturbance, especially to disturbance speed, U.

The closer this speed matches the longwave speed, *c* (i.e., the closer is the Froude number *Fr* = *U/c* to 1.0), the stronger the sea level response. Another important factor is the "fetch time", i.e., the time when the disturbance speed remains close to the resonance speed and atmospheric energy is actively accumulated by the ocean. Also, the results of numerical modelling and comparison with observations show that meteotsunamis are generated only by a specific sector of directions of incoming atmospheric waves, normally coinciding with the orientation of the inlet or bay.

(3) The combination of external and internal factors determines the individual reaction of each site to propagating atmospheric disturbances. There are some specific sites ("*hot spots*"), in particular, Ciutadella Inlet, Vela Luka Bay, Nagasaki Bay and Mazaro del Vallo (western Sicily) that have highly favourable conditions for effective generation of meteotsunamis. For this reason, meteotsunamis at these sites occur much more often, have much higher intensity and even typically have local names, specifically *rissaga, šćiga, abiki* and *marrobbio*, respectively. However, now and then hazardous meteotsunami events take place in new regions, where such events have never been reported before (like in 2014 in Odessa and in 2017 in the Persian Gulf), demonstrating the need for meteotsunami studies, even for "quiet" regions.

Numerical modelling has begun to be used ever more often to examine meteotsunamis. *Šepić et al*. [2016] numerically simulated the great event in the Adriatic Sea of 25-26 June 2014. *Kim and Omira* [2021] numerically simulated meteorological tsunamis near the coast of Portugal, and *Titov and Moore* [2021] constructed a numerical model of the extreme derecho-induced meteotsunami of 13 June 2020 on the northeast coast of the United States. The major advantage of numerical modelling of both seismically generated tsunamis and meteotsunamis is that they allow us to estimate the risk of these events in the regions where there were no actual observations, such as Boundary Bay.

Recently, *Rabinovich et al.* [2021, 2023] numerically examined meteorological tsunamis in the southern Strait of Georgia, Juan de Fuca Strait and the southwestern Vancouver Island shelf. *Rabinovich et al.* [2021] focused on the "Point Atkinson meteotsunami" of 1 November 2010, while *Rabinovich et al.* [2023] concentrated on the "Songda event" of 14-16 October 2016. The

results of numerical modelling in 2021 study, as well as in [*Rabinovich et al.*, 2023], combined with a comprehensive analysis of existing observational data enabled the authors to provide several general conclusions regarding the generation mechanisms and characteristics of meteotsunamis in this region. The numerical experiments revealed a strongly individual character to the sea level response at each site to the changing air pressure speed, direction and intensity. Each location has a set of "site-specific" air pressure characteristics that produce the strongest sea level response. More specifically, some intense atmospheric disturbances produce pronounced sea level oscillations in Patricia Bay, but do not generate noticeable oscillations at nearby Victoria. Similarly, other disturbances can induce tsunami-like oscillations at Victoria but do not trigger any sea level response in Patricia Bay. Differences in the response between sites appear to be determined by the local topography and coastline geometry.

Section 3 below uses the results of *Rabinovich et al.* [2021], but with focus on Boundary Bay.

3. NUMERICAL MODELLING OF METEOTSUNAMIS FOR THE BC COAST

To estimate maximum possible meteotsunami heights in Boundary Bay, we used an ocean model based on the depth-integrated shallow-water equations, ignoring the Coriolis effect and all non-linear terms, except bottom friction. The equations of horizontal motion (2)-(3) and continuity (4) are then as follows:

$$\frac{\partial u}{\partial t} = -\frac{C}{h^2} u\sqrt{u^2 + v^2} - gh\frac{\partial \eta}{\partial x} \tag{2}$$

$$\frac{\partial v}{\partial t} = -\frac{C}{h^2} v\sqrt{u^2 + v^2} - gh\frac{\partial \eta}{\partial y} \tag{3}$$

$$\frac{\partial \eta}{\partial t} = -\frac{\partial u}{\partial x} - \frac{\partial v}{\partial y} + \frac{\partial \zeta_A}{\partial t}, \tag{4}$$

where t is time, (x, y) are the Cartesian coordinates in the eastward and northward directions, respectively, (u, v) are the depth-integrated components of velocity in the (x, y) directions, h is the depth, g is the gravitational acceleration, η is the sea level adjusted for the equilibrium inverse

barometric (IB) effect, ζ_A is the sea level equivalent to the non-equilibrium air pressure effect, and *C* is the nonlinear bottom friction coefficient (set to 0.0025, a commonly accepted value). For wave-heights of up to 1-2 m, the difference between tsunami-like waves modelled with linear versus nonlinear equations of motion is negligible and the Coriolis force for processes on a meteotsunami/tsunami time scale can be neglected [*Kowali*k, 2012]. The effect of air pressure on sea level appears as a time derivate in the continuity equation (4). This model code had been developed by Dr. Isaac Fine (Institute of Ocean Sciences, Sidney, BC, Canada) and has been used successfully in various meteotsunami modelling experiments [cf. *Monserrat et al*., 2014; *Šepić et al*., 2018; *Rabinovich et al.,* 2020].

At the coastal boundary (*G*), we assume that there is a vertical wall with zero normal flow:

$$U_n = 0 \qquad \text{on } G, \tag{5}$$

while on the open boundary (Γ) we used the radiation condition:

$$\frac{\partial \eta}{\partial n} - \frac{1}{c}\frac{\partial \eta}{\partial t} = \frac{\partial \zeta_A}{\partial n} - \frac{1}{c}\frac{\partial \zeta_A}{\partial t} \qquad \text{on } \Gamma, \tag{6}$$

where $c = \sqrt{gh}$ is the longwave speed and *n* is directed perpendicular to the boundary Γ.

The explicit finite-difference method was used to solve equations (1)-(3) with boundary conditions (5) and (6). We applied the Arakawa C-grid approximation and used a grid with 9×6 arcsec (~180 m × 180 m) resolution. The model domain size was 1379 x1319 grid points (Figure 4a). Within the constraints of the Courant-Friedrichs-Lewy (CFL) criterion, the time step (Δt) was chosen to be 1.1 s.

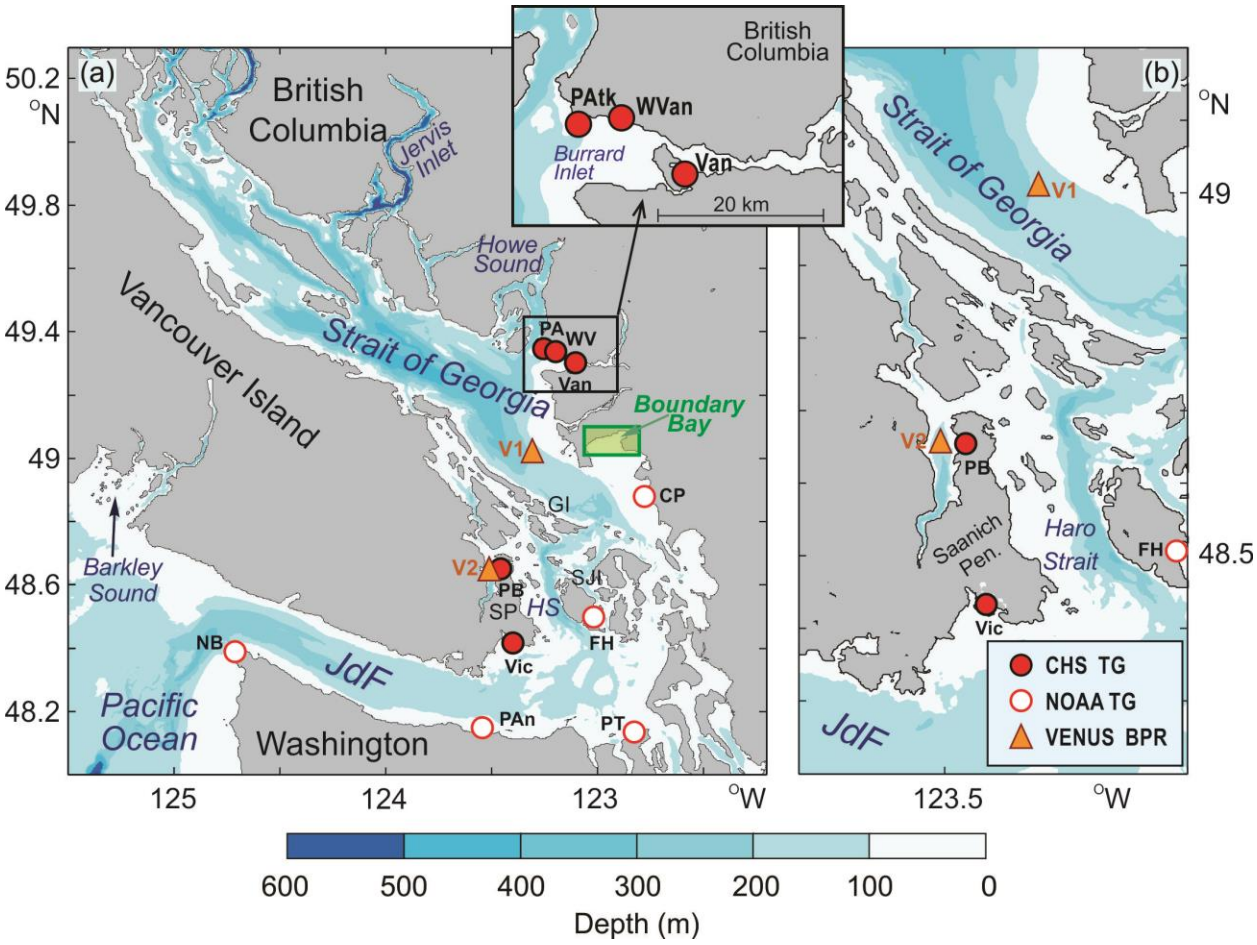

Figure 4. (a) Map of the southern Strait of Georgia and Juan de Fuca Strait (JdF) showing locations of the Canadian Hydrographic Service (CHS) and the US National Oceanic and Atmospheric Administration (NOAA) coastal tide gauges (TGs). Also are shown the locations of two Ocean Network Canada (ONC) VENUS bottom pressure recorders (BPR); and Boundary Bay (the *green box*). (b) An expanded version of (a) for the area of the Saanich Peninsula, Saanich Inlet (SI), Haro Strait (HS), the Gulf Islands (GI) and the San Juan Islands (SJI). Other abbreviations are: "PA" and "PAtk" = Point Atkinson, "WV" and "WVan" = West Vancouver, "Van" = Vancouver, "PB" = Patricia Bay, "Vic" = Victoria, "NB" = Neah Bay, "PAn" = Port Angeles, "PT" = Port Townsend, "FH" = Friday Harbor and "CP" = Cherry Point.

In our numerical experiments, the model was forced by a "bell-shaped" travelling air pressure disturbance of the form (1), where A = 3 hPa is the disturbance amplitude, a = 5 min is the half-width of the disturbance, and $\gamma = a/b$ is the slope parameter, where b = 100 seconds is the half-width of the increasing (decreasing) part of the pressure impulse. This function fits the air pressure

changes of about ~3 hPa/10 min and has been successfully used for modelling other meteotsunami events [cf. *Šepić et al.,* 2018]. We undertook three types of general model experiments:

(1) Four model runs with the speed and direction of propagation set to match the estimated propagation parameters of disturbances D1-D4 (Table 1) that were adopted from *Rabinovich et al.* [2020]. These disturbances were observed to propagate over the study region on 1 November 2010. The cross-propagation width of the disturbances spanned the entire computational domain.

Table 1. Main characteristics of the four air pressure disturbances observed over Vancouver Island on 1 November 2010. Here, "height" corresponds to the trough-to-crest range in pressure.

Disturbance	Time (UTC)	Area	Period (min)	Height H_{max} (hPa)	Rate, C_{max} (hPa/5 min)	Type
D1	5:30 – 8:30	Tofino, Strait of Georgia	150	1.1	0.7	Single
D2	6:00 – 8:00	Saanich Peninsula	40	1.3	0.8	Single
D3	14:00 – 17:30	Strait of Georgia	15 – 60	3.0	2.0	Multiple
D4	14:00 – 22:00	Saanich Peninsula	15 – 100	2.1	1.7	Multiple

(2) Sensitivity analysis of sea level response to changing air pressure parameters. A series of numerical experiments (model "runs") were done for four selected sites on the coasts of British Columbia (BC) and Washington (WA) - Patricia Bay, Point Atkinson, Port Angeles and Friday Harbor. A similar numerical modelling approach was used by *Orlić et al.* [2010] to examine the catastrophic flood of 21 June 1978 in Vela Luka Bay in the Adriatic Sea and by *Šepić et al.* (2018) to examine the "Odessa tsunami" of 27 June 2014 in the Black Sea. These studies indicated that the most important tsunamigenic air pressure (AP) parameters are the speed and direction of the disturbance propagation.

(3) More general numerical experiments were conducted in order to identify "hot spots" [*Šepić and Rabinovich*, 2014] in the region under study and "hot parameters" of the propagating disturbances.

In Section 4, we present the results of specific numerical experiments for Boundary Bay in order to identify parameters of the propagating disturbances (speed and direction) that can produce maximum meteotsunami wave heights and ocean currents in the study region. Our numerical experiments used a bell-shaped air pressure disturbance propagating over the computational domain (Figure 1a) with predefined speeds and directions.

3.1. "BELL-SHAPED" NUMERICAL EXPERIMENTS

For the bell-shaped disturbance, with given propagation speeds and directions, the largest simulated oscillations were found to reach wave-heights (range) of up to 120 cm along the southern coast of Vancouver Island (northern part of Juan de Fuca Strait), when the disturbance was set to propagate with the D1 speed (~28 m/s) toward the northeast direction. In contrast, the smallest oscillations, with simulated wave-heights of up to 64 cm, occurred for the wave speed of 20 m/s and direction of 96° True associated with the D3 disturbance.

In general, the results of our numerical modelling for southern British Columbia and northern Washington (excluding Boundary Bay) indicate that the disturbances moving across the Strait of Georgia (i.e., northeastward) at relatively high speeds (26-28 m/s) produce much stronger meteotsunamis than those propagating eastward at slower speeds (20 m/s) (Figure 5). Specific locations ("hot spots") along the coasts of the Strait of Georgia, Juan de Fuca Strait and the outer coast of Vancouver Island were found to be prone to potentially destructive meteotsunami wave heights. These locations are: (1) the southeast coast of Barkley Sound (see Figure 4) and adjacent southwest coast of Vancouver Island; and (2) the easternmost part of Juan de Fuca Strait, including the southern coasts of the Saanich Peninsula and the San Juan Islands (Figure 5). A strong sea level response to these disturbances was also observed at (3) the head of Howe Sound. In contrast, the Boundary Bay region seems to be shielded from extreme longwave sea level oscillations arriving from the open sea by a very shallow and wide shelf area that effectively reflects the shoreward propagating waves (see Figure 1 for all locations). As a consequence, there is a strong similarity with landslide-generated tsunamis simulated for this region [*Rabinovich et al.,* 2003], which were also found to be effectively reflected by the shallow shelf bordering the eastern coast of the southern Strait of Georgia.

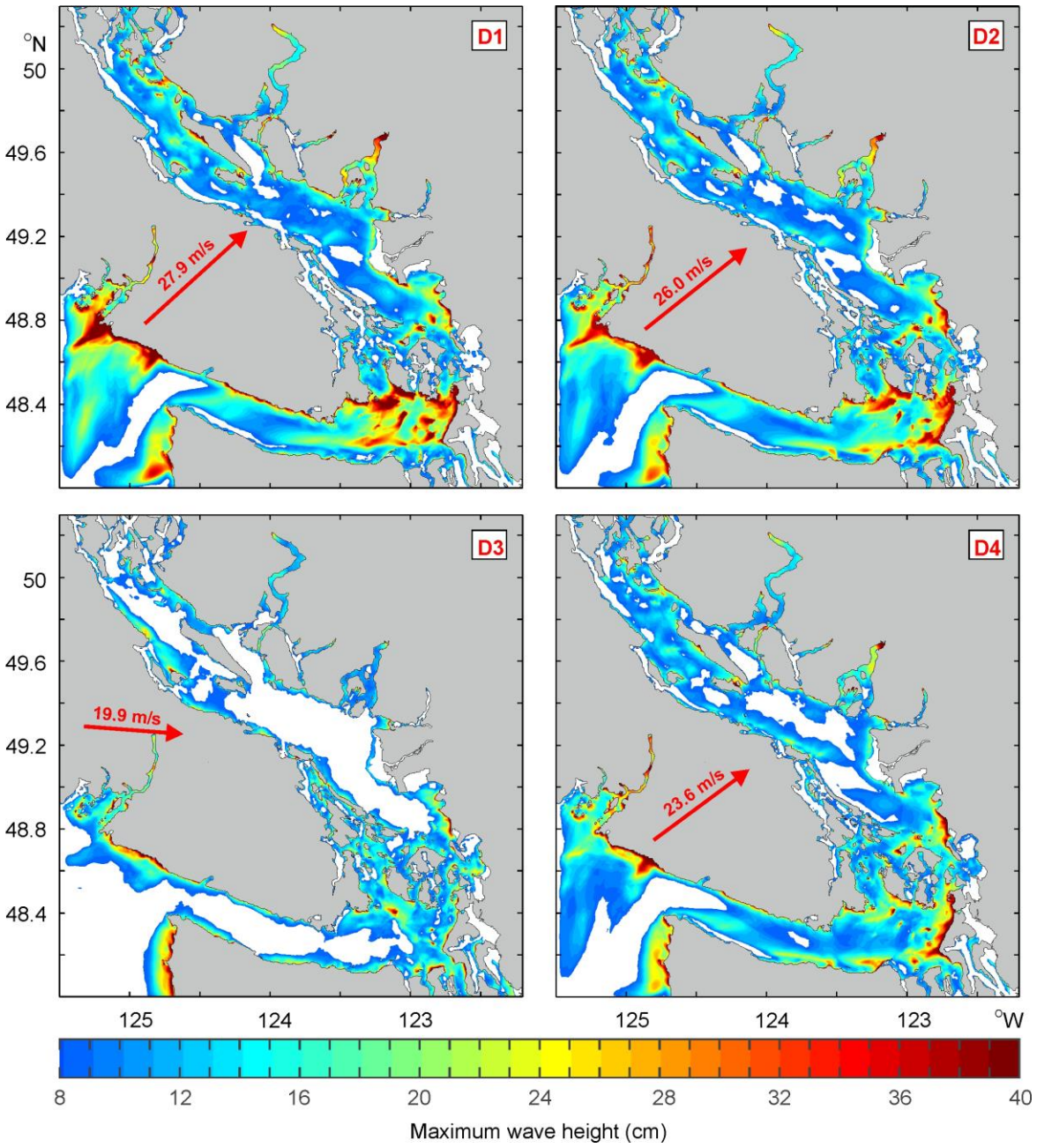

Figure 5. Maximum wave amplitudes obtained in numerical experiments based on an atmospheric bell-shaped disturbance propagating with the estimated velocities of the D1-D4 disturbances.

Simulations of the meteotsunami waveforms generated by the bell-shaped disturbance propagating with the D3 velocity are shown for four BC tide gauge sites, two VENUS BPR stations and Washington mainland station Cherry Point, while those for the bell-shaped disturbance

propagating with the D4 velocity are shown for Patricia, VENUS BPR V2 (Saanich Inlet), Victoria and four Washington tide gauge sites (Figure 6; see Figure 4 for locations). The computed wave amplitudes for the SoG stations (Figure 6a) generated by the bell-shaped disturbance propagating with the D3 velocity were 8-12 cm at the three BC mainland coastal stations and about 5 cm at the two BPRs. The highest and most impulsive-like waveforms were obtained for Patricia Bay and Cherry Point, where the simulated oscillations had a trough-to-crest height of 26 and 25 cm, respectively, i.e., much higher than the measured wave amplitudes. There are two possible reasons for the poor agreement between the computed and observed waveforms at these stations: (1) the spatial resolution (180 m) of the model is too coarse to allow for accurate reproduction of the real bathymetry and coastal geometry in the corresponding regions, and consequently, for the model to simulate eigen (resonant) oscillations in local basins; and (2) the inability of the idealized bell-shape function used for forcing the ocean model to simulate the actual air pressure disturbance, both in the term of its shape and propagation parameters. On the other hand, the model reproduces the wave amplitudes and arrival times at these three coastal stations and at two VENUS BPRs reasonably well.

Most of the JdF group of stations (including Patricia Bay and VENUS V2 stations) for the bell-shaped disturbance propagating with the D4 velocity had computed wave heights of 13-18 cm (Figure 6b). The exceptions, as well as for the D3 disturbance (Figure 6a), were Patricia Bay located in Saanich Inlet, southeast Vancouver Island, and Cherry Point located on the mainland coast to the south from Boundary Bay, where the simulated meteotsunami wave heights reached 37 and 35 cm, respectively, and had an impulse-like beginning (Figure 6b). In the general map of maximum computed wave amplitudes for the D4 disturbance (Figure 5, right bottom plot), it is evident that these regions, together with the coastal region westward from the Puget Sound entrance, are areas of strongly amplified waves. However, these results are different from the observed heights [*Rabinovich et al.*, 2020], which had maximum meteotsunami wave amplitudes at Port Angeles and Victoria. The simulated record for VENUS V2 has a similar impulse-like first wave that is absent in the observed record at this station, but the rest of the actual record is reproduced fairly well. The encouraging result is that the first couple of hours of the sea level records for stations Victoria and Port Townsend are also reproduced well, and for Friday Harbor and Port Angeles the model also gives reasonable results. However, after the first two hours, the agreement becomes much worse.

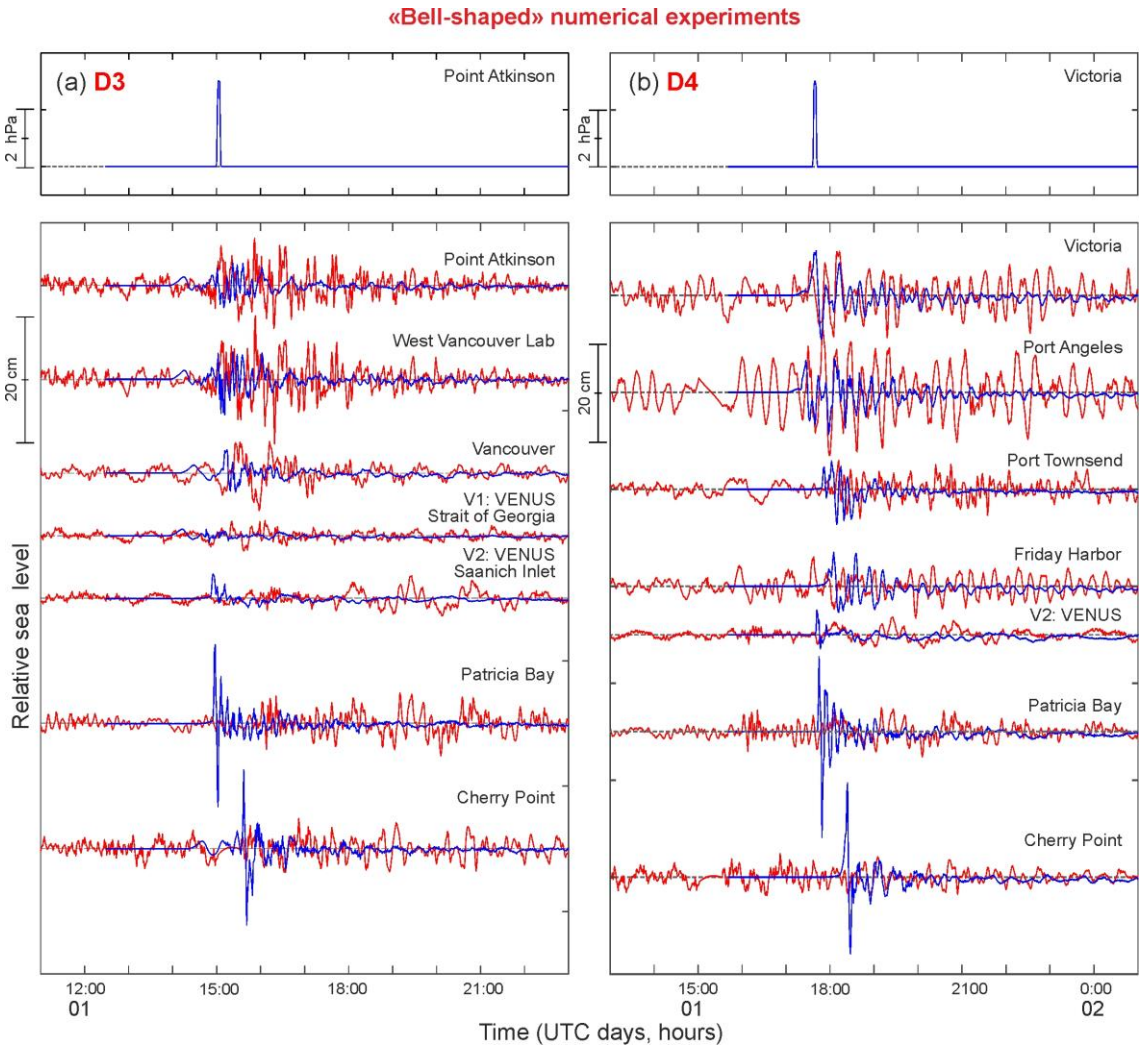

Figure 6. Measured (red) and computed (blue) meteotsunami waveforms at tide gauge and BPR locations. In the numerical experiments, sea levels oscillations were forced by propagating bell-shaped atmospheric disturbances of unlimited cross-propagation width (upper panels) with velocity parameters of (a) D3 for the Strait of Georgia and (b) D4 for Juan de Fuca Strait.

3.2. SENSITIVITY ANALYSIS AND SEA LEVEL RESPONSE TO AIR PRESSURE SPEED AND DIRECTION

The analyses of the 2010 Point Atkinson meteotsunami event presented in the previous sections raises several questions:

- *How sensitive is the sea level response to air pressure disturbance parameters?*

- *What are the resonant (most effective) disturbance parameters that produce the strongest sea level oscillations along the coast?*

In response to these questions, we selected four sites on the coasts of BC and WA - Patricia Bay, Point Atkinson, Port Angeles and Friday Harbor - and for each of the sites provided a series of numerical experiments ("runs"). A similar numerical modelling approach was used by Orlić et al. (2010) to examine the catastrophic flood of 21 June 1978 in Vela Luka Bay in the Adriatic Sea and by Šepić et al. (2018) to examine the "Odessa tsunami" of 27 June 2014 in the Black Sea. As noted earlier, these studies indicate that the most important tsunamigenic air pressure (AP) parameters are the speed and direction of the disturbance propagation.

Our numerical experiments used a bell-shaped air pressure disturbance propagating over the computational domain (Figure 4a) with predefined speeds and directions. The main purposes of these experiments were:

(1) To identify the specific parameters of the propagating air pressure disturbance producing the strongest sea level response to the atmospheric forcing for four selected sites.
(2) To estimate how close were these parameters to the actual parameters of the D3 and D4 disturbances propagating over the region on 1 November 2010.
(3) To estimate how sensitive are the results to changes in the velocity parameters of the propagating disturbance.

The disturbance propagation velocity parameters were chosen to vary in the following ranges:

- Speed: from 14 to 41 m/s, with an increment of 3 m/s;
- Direction: from 20º to 110º True, with an increment of 10º (i.e., the disturbances propagated mainly toward the northeast or east).

The results of runs consisting of combination of 10 different speeds and directions (= 100 numerical experiments) shown in Figure 7 enable us to better understand the generation mechanism of meteotsunamis in this region and to arrive to several principal conclusions about this phenomenon.

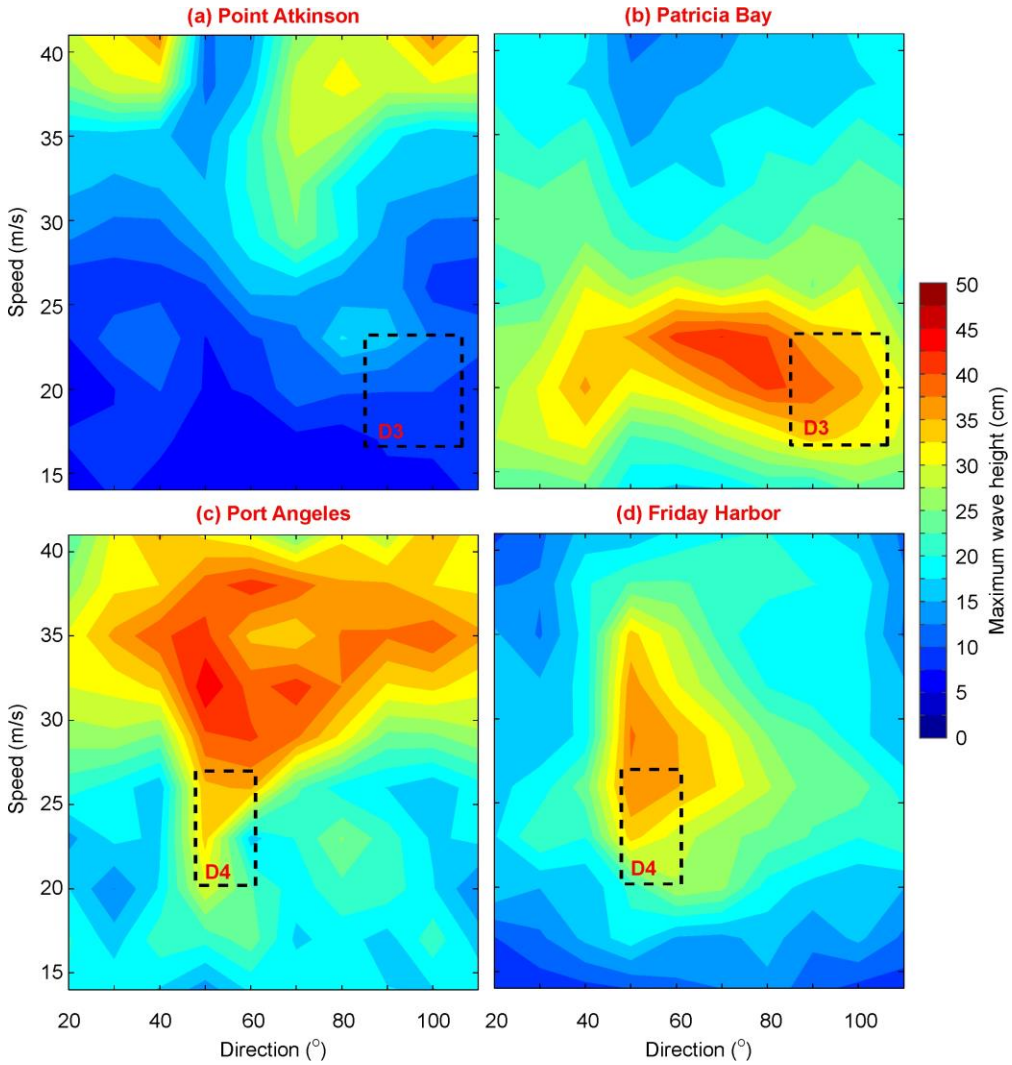

Figure 7. Maximum simulated wave amplitudes as functions of speed and direction of a propagating bell-shaped disturbance, at: (a) Point Atkinson; (b) Patricia Bay; (c) Port Angeles; and (d) Friday Harbor. Dashed boxes span regions in speed-direction space of the most likely values for (a,b) disturbance D3 and (c,d) disturbance D4.

(1) The most important feature evident from these experiments is the markedly individual character of the sea level response at each site; in particular, the air pressure velocity parameters that induce pronounced oscillations at Point Atkinson do not generate noticeable oscillations at Patricia Bay or Friday Harbor, and *vice versa* (Figure 7). It appears that each site has a specific set of "hot" air pressure parameters producing the strongest sea level response. We found this for the four selected sites, but it appears that the same is true for other sites.

(2) The numerical experiments show that the sea level responses are highly sensitive to the disturbance parameters, especially the disturbance speed. For example, a disturbance moving eastward with a speed of 40 m/s generates sea level oscillations of almost 40 cm at Point Atkinson, while the same disturbance propagating with a speed of 20 m/s produces wave heights of < 5 cm (Figure 7a). For Patricia Bay, the opposite occurs, whereby a disturbance propagating with a speed of 20 m/s generates sea level heights of ~45 cm, whereas a disturbance with a speed of 40 m/s generates heights of <10 cm (Figure 7b). Changes in sea level associated with changes in the disturbance direction are less variable. For example, at Patricia Bay and Port Angeles, the generated wave heights are almost the same over a wide range of directions of 30-100º (Figure 7b,c). In contrast, at Point Atkinson and Friday Harbor, the sea level response is much more selective, with maximum sea level heights occurring within two narrow beams centered around ~35º and 100º True at the first station (Figure 7a) and near 50-65º True at the second (Figure 7d). The indication is that differences for individual sites are determined by the local topography and coastline geometry.

(3) The observed D3 parameters (the disturbance direction and speed) are relatively close in value to the "hot" (most effective) air pressure parameters obtained for the Patricia Bay sea level simulations (Figure 7b), while the observed D4 parameters are similar to the effective parameters for the Port Angeles and Friday Harbor sea level simulations (Figures 7c,d). This means that such disturbances can produce significant oscillations at these stations.

Next, we show, in greater detail, results of the sensitivity study to variations in the disturbance parameters for six stations of the SoG group and five stations of the JdF group (except Neah Bay) (Figure 8). For "reference parameters", we selected the D3 speed (20 m/s) and direction (100º True) for the first group and the D4 parameters (23 m/s and 50º True) for the second. We fixed one of these parameters and varied the others (speed from 14 to 41 m/s and direction from 20º to 110º True). As revealed by Figure 8, these results are consistent with the above findings, namely that the proximity of the speed of the atmospheric disturbance to the Proudman resonance speed [*Proudman*, 1929] plays a much more important role (at least for this region) than the disturbance direction. Also, according to these experiments, the sea level response at Patricia Bay is considerably stronger than at other stations.

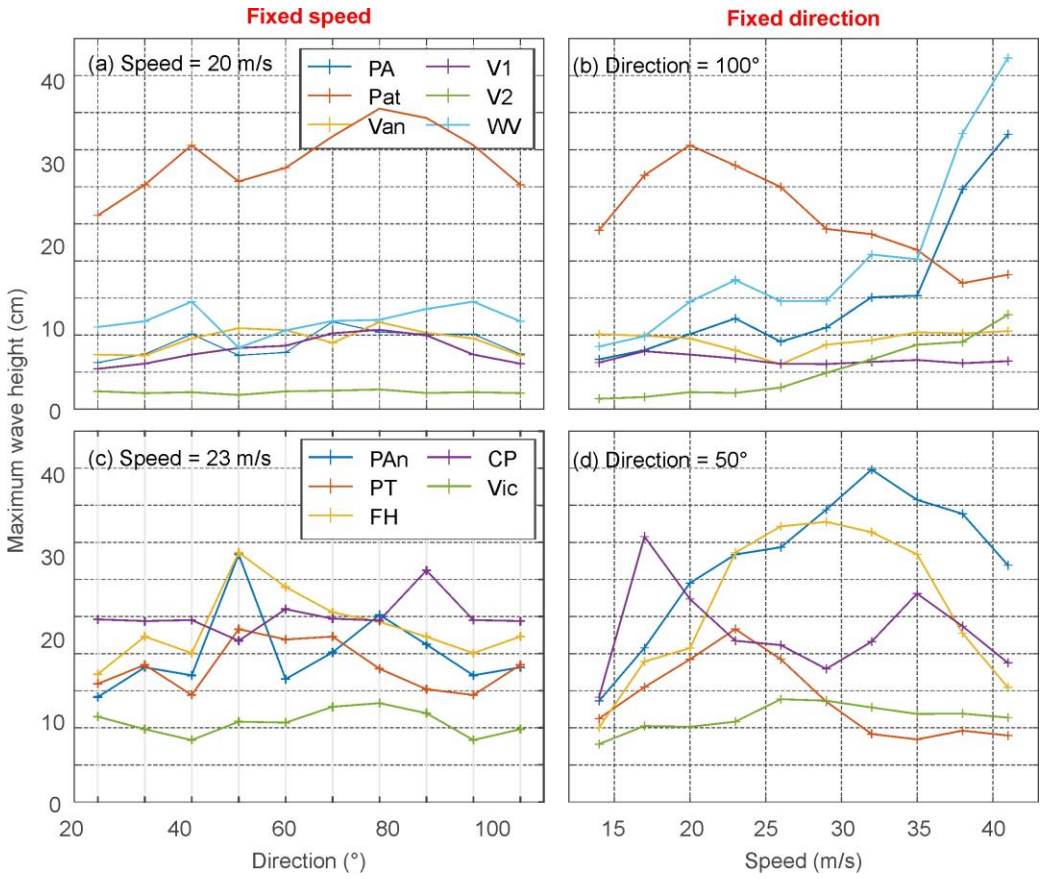

Figure 8. Maximum simulated wave amplitudes for the bell-shaped atmospheric pressure disturbance as a function of: (a) a fixed speed of 20 m/s and variable direction; (b) a fixed direction of 100° True and variable speed; (c) a fixed speed of 23 m/s and variable direction; and (d) a fixed direction of 50° True and variable speed. Fixed values are chosen to represent the propagation parameters of the (a, b) disturbance D3; and (c, d) disturbance D4. PA = Point Atkinson, Pat = Patricia Bay, Van = Vancouver, V1 and V2 = VENUS BPR stations, WV = West Vancouver, Pan = Port Angeles, PT = Port Townsend, FH = Friday Harbor, CP = Cherry Point, and Vic = Victoria.

3.3. EFFICIENCY OF METEOTSUNAMI GENERATION

In Subsection 3.2, we noted that the sea level response to propagating air pressure (AP) disturbances strongly depends on the disturbance velocity. In general, these results are understandable considering the principal role that Proudman resonance has been shown to play in meteotsunami formation in various regions of the world oceans; i.e., the coincidence of the propagation speed of the atmospheric disturbance and the speed of long ocean waves [cf. *Šepić et*

al., 2016; *Rabinovich,* 2020]. The closer is the speed of the atmospheric waves to the mean longwave speed in a specific region, the stronger is the sea level response. The disturbance propagation direction determines if the waves arriving from the open ocean are favourably oriented along the axis of the basin, where they are amplified through the funnelling and other effects. In the present subsection, we consider results from more general numerical experiments in order to identify "hot spots" [*Šepić and Rabinovich*, 2014] in the region under study and "hot parameters" of the propagating disturbances.

For these numerical experiments, we selected six sites: Point Atkinson (PA), West Vancouver (WV), Patricia Bay (PB), Victoria (Vic) (all BC), Cherry Point (CP) and Port Angeles (PAn). The computational domain and location of the stations are shown in Figure 1a. In these experiments, we propagated the bell-shaped air pressure disturbance over the region with predefined speeds and directions. The model was the same as described in Subsection 3.1. A wide range of disturbance speeds was considered, from 10 to 70 m/s, with an increment of 5 m/s, along with a full circle of propagation directions, with azimuths from 0º to 360º True and an increment of 10º (as per standard meteorological convention, the disturbances propagate **from** the directions specified). As revealed by Figure 9, the main computational findings are:

- All four stations located in the southern Strait of Georgia or vicinity (PA, WV, PB and CP) had similar sea level responses, consisting of relatively large meteotsunamis produced by disturbances propagating from the east-southeast. At stations PA and WV, the strongest response occurred for disturbances propagating with a speed of 50-60 m/s (which seems unrealistically fast), while at stations PB and CP, the maximum response was for speeds of 20-35 m/s. The latter values are very close to the D3 and D4 air pressure disturbance speeds, which would explain the large computed wave heights at these stations (Figure 5).
- The enhanced response at Victoria also corresponds to disturbances coming from E-SE. However, this station looks "cold" (Figure 9), probably because the model grid resolution was not sufficient to account for local resonant effects at this station [cf. *Rabinovich et al.*, 2003].
- Port Angeles has the strongest response of the five stations examined. Here, a disturbance propagating from the NE (25º-60º True) with a speed of about 30 m/s will produce a meteotsunami with a wave amplitude in excess of 80 cm. However, an air pressure

disturbance from this direction is very rare; most disturbances in this region propagate from NW to W to S [cf. *Thomson et al.*, 2009].

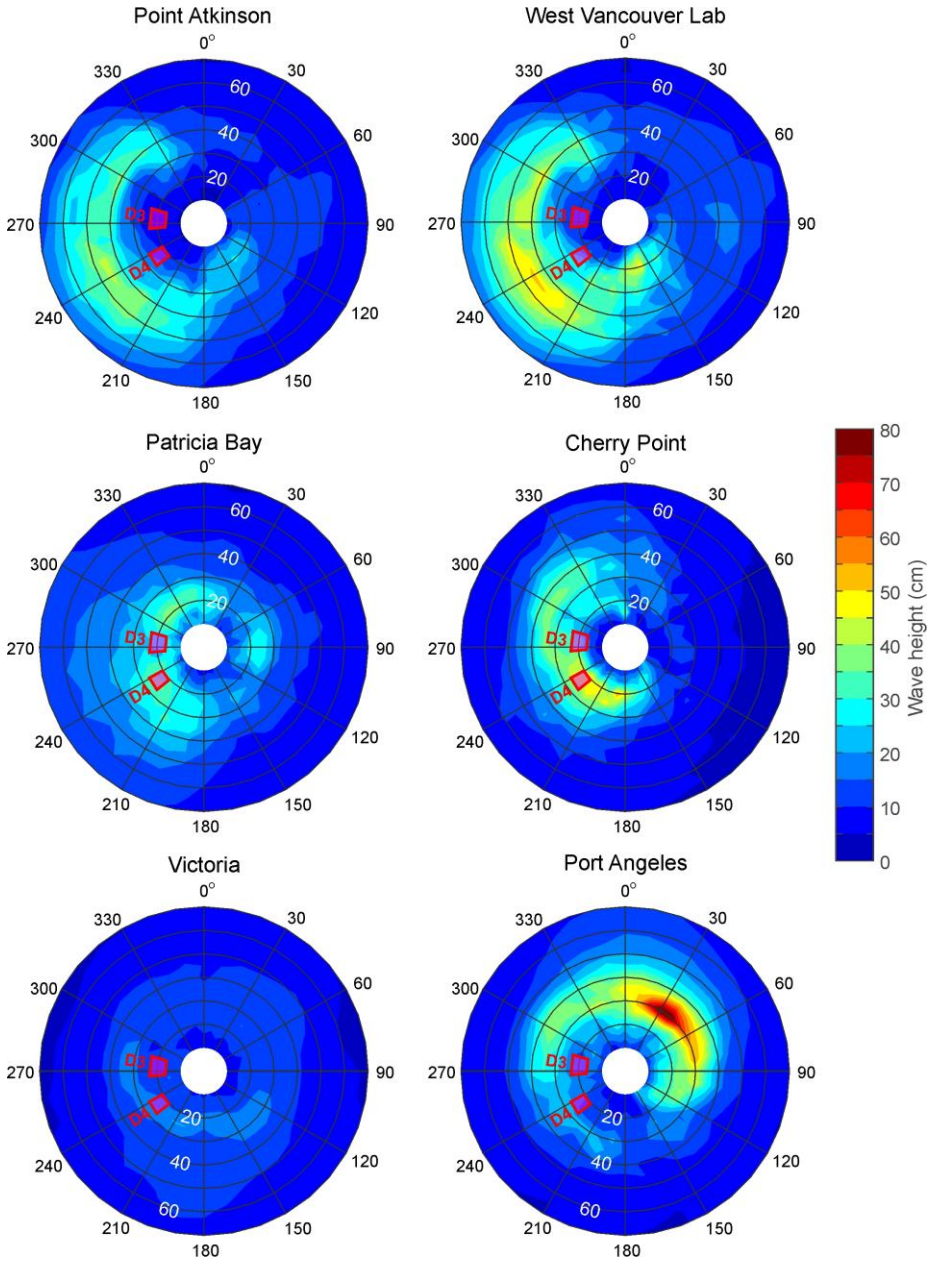

Figure 9. Maximum simulated wave amplitudes as functions of speed (range 10–70 m/s) and direction (range 0º-360º True) for a propagating bell-shaped disturbance impacting Point Atkinson, West Vancouver, Patricia Bay, Cherry Point, Victoria and Port Angeles. Red trapezoidal boxes span areas in speed-direction space having the most likely values for disturbances D3 and D4. The disturbance directions are shown as the direction from which the disturbance is propagating, e.g. the shown direction of 225º True means that this disturbance was propagating from the SW toward the NE.

4. NUMERICAL MODELLING OF METEOTSUNAMIS IN BOUNDARY BAY

The numerical model described in Section 3 was next used to simulate meteotsunamis in Boundary Bay. We selected 12 computational sites: three (1-3) on the coast of Boundary Bay and nine more (4-12) in open water (Figure 10). For these sites, we computed sea level elevations and current velocities and estimated their extreme values. In these experiments, we propagated the bell-shaped air pressure disturbance over the region with predefined speeds and directions.

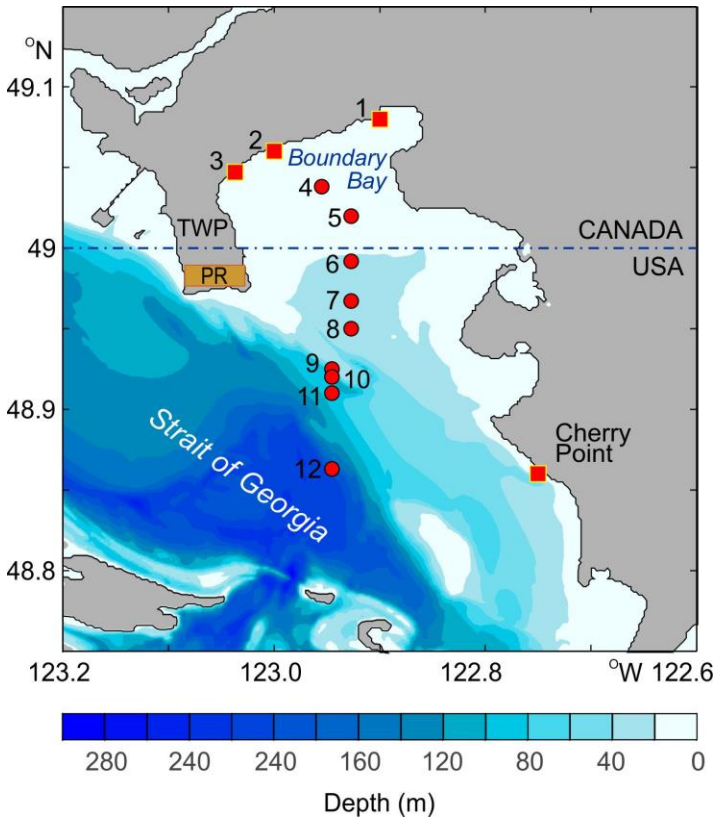

Figure 10. Map of the southern Strait of Georgia including Boundary Bay. Numbers 1-12 denote the points used for model outputs; the squares are coastal sites and circles are the open-water sites. "TWP" = the Tsawwassen Peninsula, "PR" = Point Roberts (highlighted in colour).

4.1. COMPUTATION OF MAXIMUM SEA LEVELS IN BOUNDARY BAY

A wide range of disturbance speeds was considered, from 10 to 70 m/s, with an increment of 5 m/s, along with a full circle of direction-from propagation directions, with azimuths from 0º to

360º True and an increment of 10º. The results of the computations are shown in Figure 11 and presented in Table 2. Our main findings are the following:

- The sea level response at the three sites located on the coast of Boundary Bay (Sites 1-3) is very small, mostly <4-6.5 cm for any disturbance direction or speed. The maximum oscillations (5.5 – 6.5 cm) are related to the southwesterly sector of directions: ~210° True (Figure 11). As indicated in Subsection 3.1, it appears that shallow and wide shelf area (Figure 10) protects the Boundary Bay region from extreme long waves arriving from the southern Strait of Georgia and hinder the coastal area from formation of major meteotsunamis.
- The sheltering effect of the shelf is evident from Table 2, which shows that the maximum amplitudes of the oscillations effectively increase in the offshore direction, ranging from 5-6.5 cm on the shoreline, to 9.6 cm at Site 4, 21.5 cm at Site 5, and 30.8 cm at Site 6 (the shelf-break). The maximum amplitude (51.3 cm) occurs at Site 9, at the entrance to the bay (Figure 10).
- The forced (atmospherically-induced) sea level oscillations incoming from the open part of the southern Strait of Georgia first increase with decreasing depth, from 33.0 cm at Site 12 to 51.3 cm at Site 9, and then attenuate rapidly over the shallow shelf area adjacent to Boundary Bay.

In general, the meteotsunami response in Boundary Bay stands in marked contrast to other regions known for regular destructive events. For Ciutadella Harbour (Spain), Vela Luka and Stary Grad (Croatia) and Nagasaki Bay (Japan), the shape of the particular bay or harbour is the main factor causing amplification of the arriving waves, whereas the coastal geometry and local bathymetry of Boundary Bay strongly attenuate the incoming waves, thereby protecting the region from significant meteotsunamis.

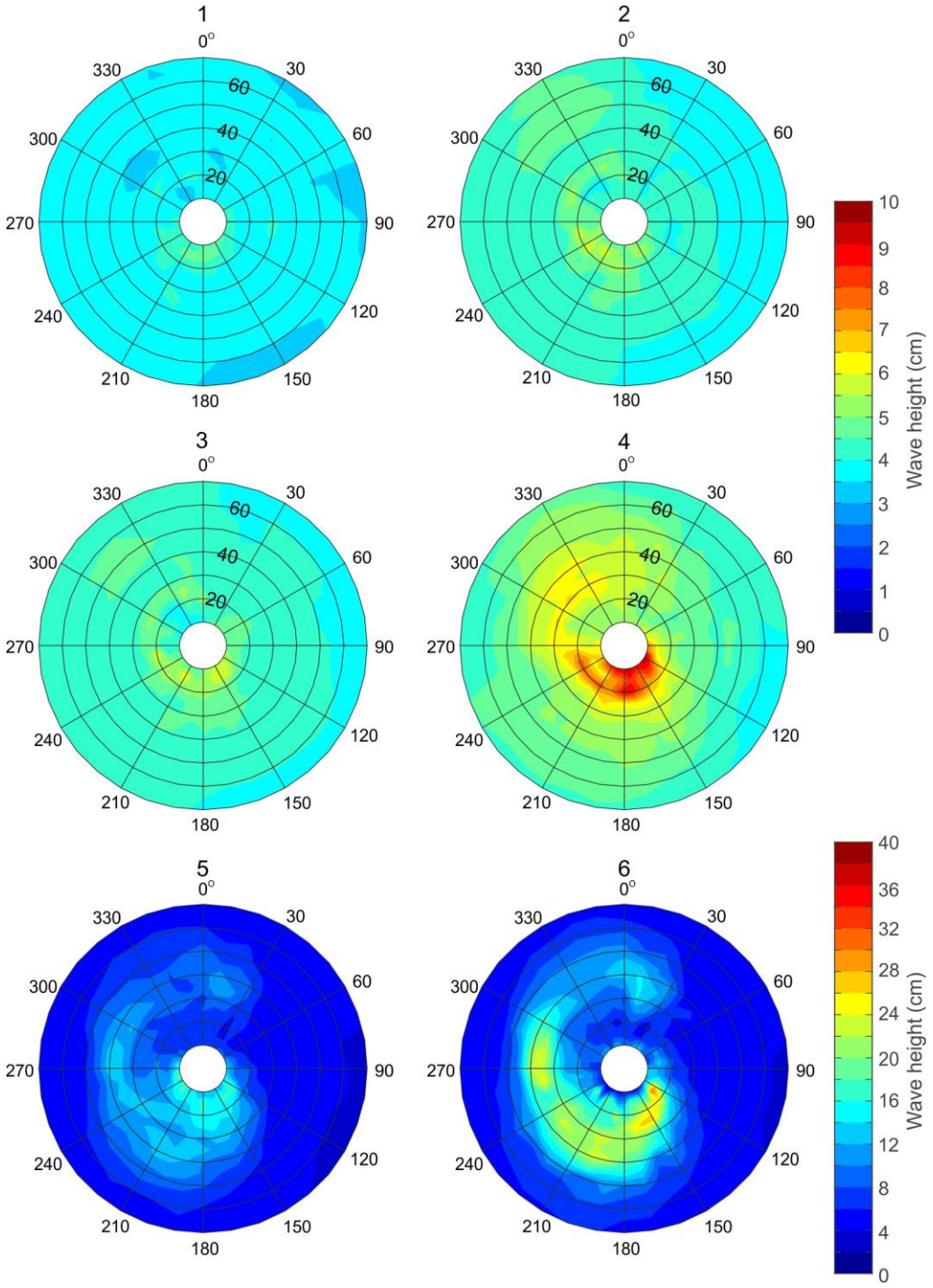

Figure 11. Maximum simulated wave amplitudes as functions of the disturbance speed (range 10–70 m/s) and direction (range 0º-360º True) for a propagating bell-shaped disturbance impacting 12 sites shown in Figure 10. The disturbance directions are shown in the conventional manner for wind (i.e., direction the wind is from)**.** For the shown direction of 225º True, the disturbance propagates from the SW toward the NE.

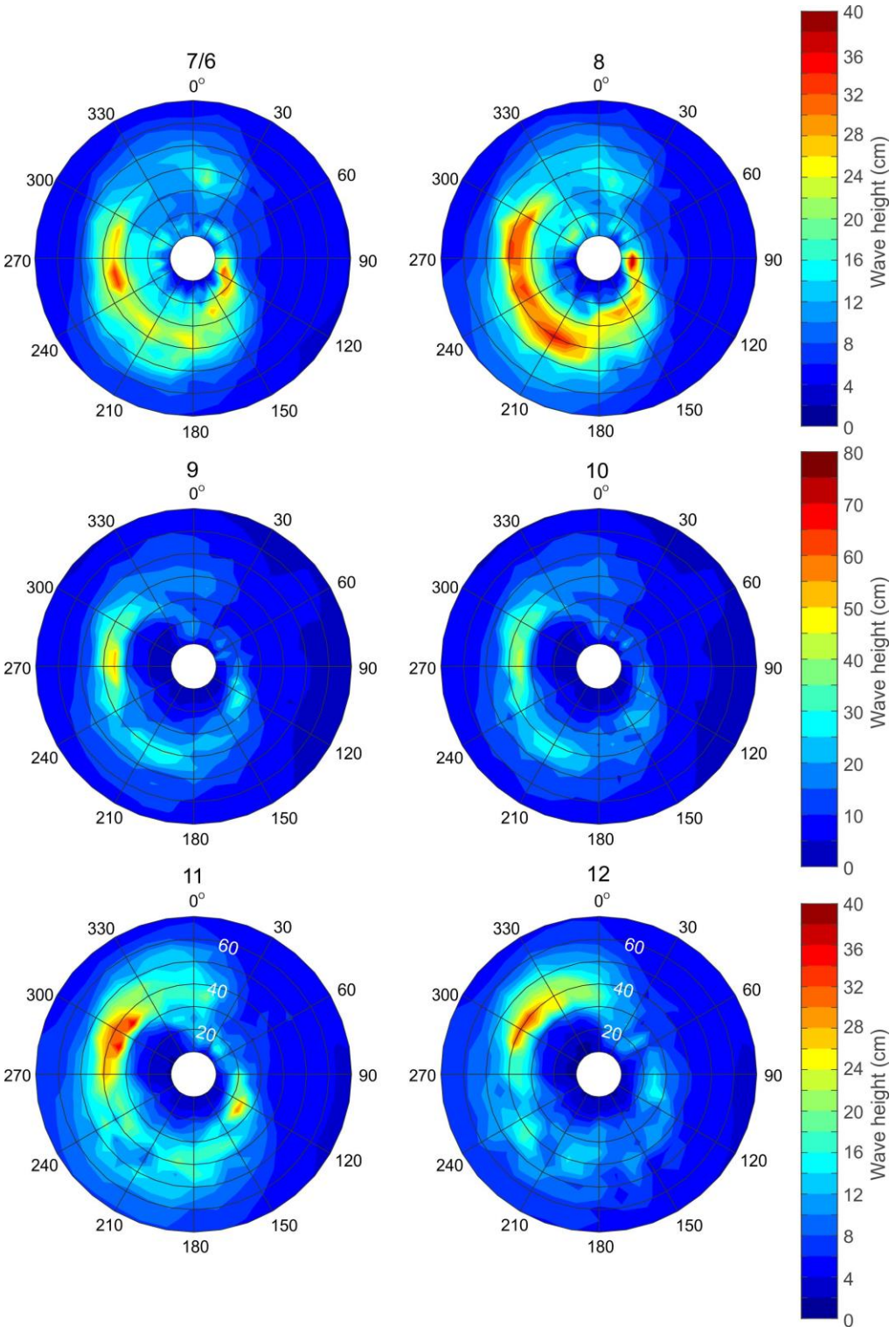

Figure 11. Continued

Table 2. Maximum computed meteotsunami wave amplitudes at 12 sites shown in Figure 10. The disturbance directions are in the direction from which the disturbance is arriving.

Point	Region	Maximum wave amplitude (cm)	Disturbance characteristics	
			Speed (m/s)	Direction (°True)
1	Coastal	4.89	15	210
2	Coastal	6.18	15	210
3	Coastal	6.56	15	210
4	Open water	9.60	10	120
5	Open water	21.49	10	250
6	Open water	30.82	15	130
7	Open water	33.74	35	260
8	Open water	38.70	15	90
9	Open water	51.33	35	260
10	Open water	43.84	35	260
11	Open water	37.22	35	310
12	Open water	33.04	40	310

4.2. COMPUTATION OF MAXIMUM CURRENT VELOCITIES IN BOUNDARY BAY

As with the case for maximum wave amplitudes, we computed the maximum current velocities in Boundary Bay using the range of disturbance speeds from 10 to 70 m/s with an increment of 5 m/s and propagation directions from 0º to 360º True with an increment of 10º. The results of the computations are shown in Figure 12 and Table 2. The main findings are:

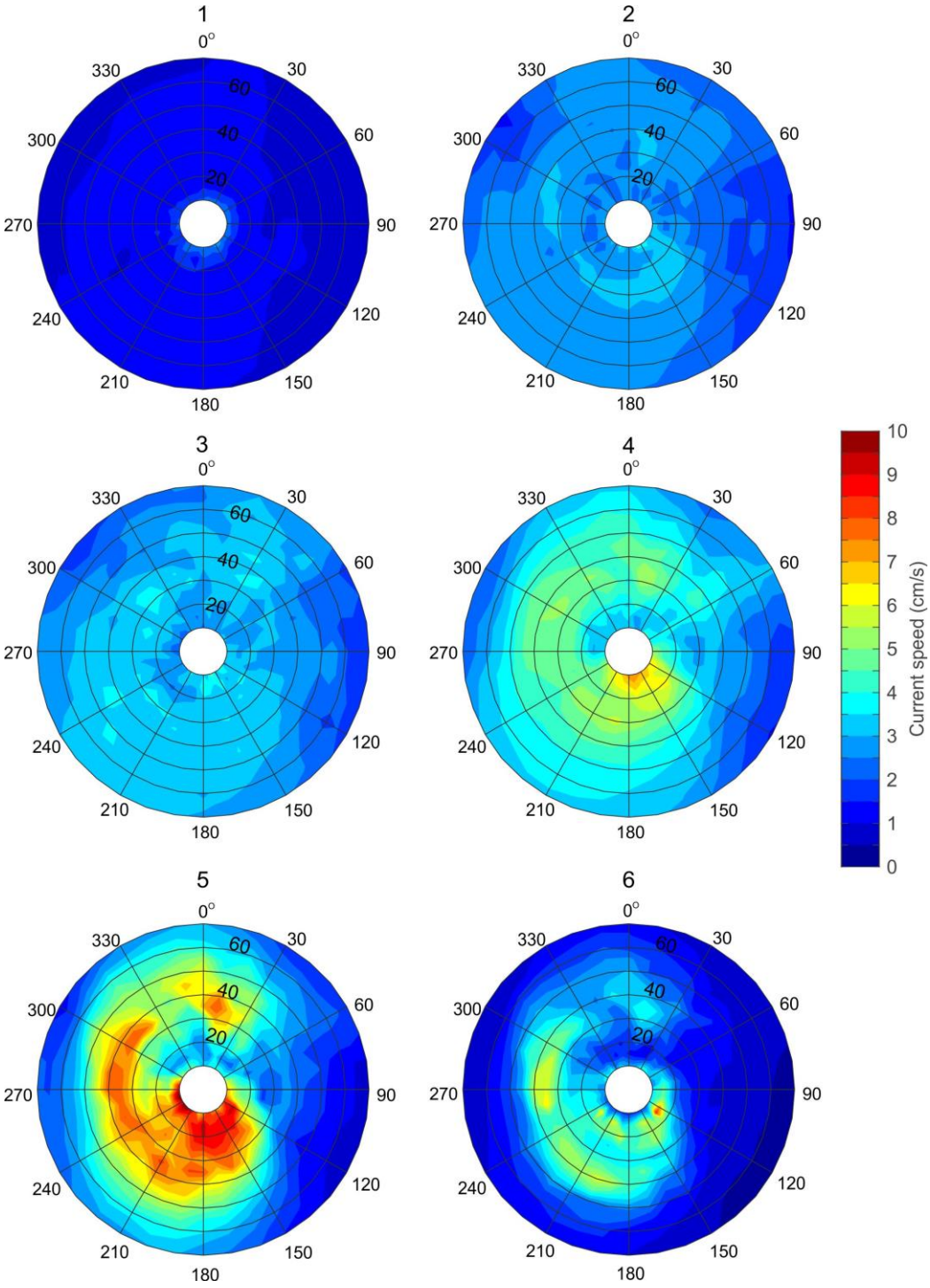

Figure 12. Maximum simulated current velocities as functions of the disturbance speed (range 10–70 m/s) and direction (range 0º-360º True) for a propagating bell-shaped disturbance impacting 12 sites shown in Figure 10. The disturbance directions are shown in the direction from which they are coming. A direction of 225º True means that the disturbance propagates from the SW toward the NE.

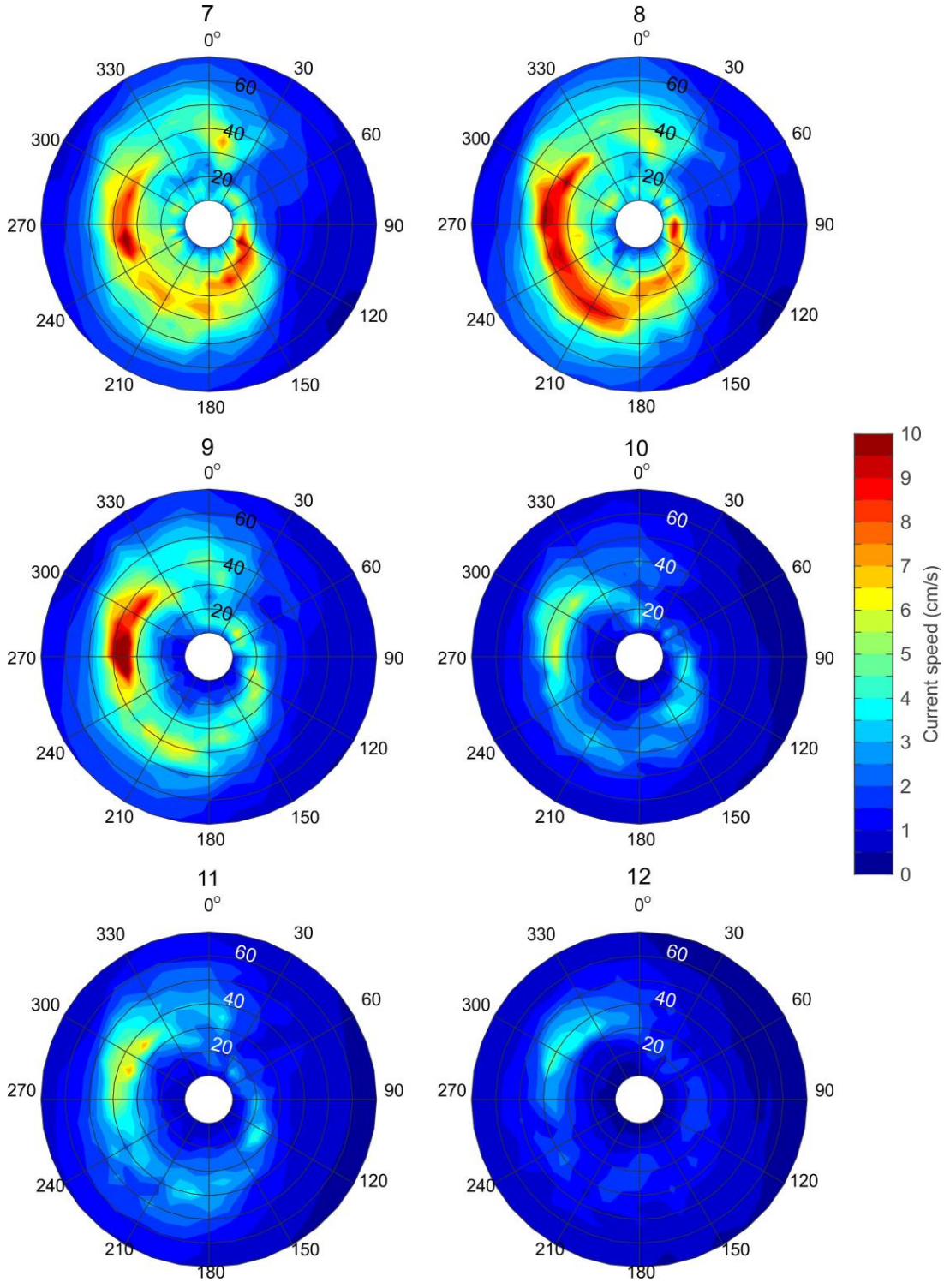

Figure 12. Continued

Table 3 Maximum computed meteotsunami current velocities at the 12 sites shown in Figure 10. The disturbance directions are in the direction from which the disturbance is arriving**.**

Point	Region	Maximum current		Disturbance characteristics	
		Speed (cm/s)	Direction (°True)	Speed (m/s)	Direction (°True)
1	Coastal	2.9	308.0	10	140
2	Coastal	4.0	315.9	10	140
3	Coastal	5.0	295.5	10	160
4	Open water	7.4	135.5	10	170
5	Open water	11.02	229.16	10	250
6	Open water	8.53	154.34	15	130
7	Open water	10.78	35.05	35	260
8	Open water	10.14	231.38	35	300
9	Open water	11.50	67.03	35	280
10	Open water	6.11	88.94	35	280
11	Open water	7.22	267.26	35	310
12	Open water	4.67	98.15	40	290

- Near the coast (Sites 1-4), maximum currents are quite small at 2.5-7.5 cm/s. Such currents are not hazardous to coastal infrastructure.
- The maximum current speeds of 10-11.5 cm/s occur at Sites 5, 7, 8 and 9 (Table 3). All of these sites are located along the axis of a small north-south oriented canyon (Figure 10).
- At deeper sites (9, 10, 11 and 12), the current speeds are strongly attenuated, from 11.5 cm/s at Site 9 to 4.7 cm/s at Site 12 (Table 3).
- As indicated by Figure 12 and Table 3, maximum current speeds are associated with atmospheric disturbances moving from the west (240 -320º True), the most common directions of propagating disturbances [cf. *Rabinovich et al.*, 2020]. In contrast, easterly disturbances produce the lowest sea level responses (Figure 11) and the weakest currents (Figure 12).

In general, meteotsunami-generated currents for the Boundary Bay region are weak and not a serious hazard.

4.3. COMPUTATION OF THE SPATIAL STRUCTURE OF COMPUTED SEA LEVELS AND CURRENTS IN BOUNDARY BAY

Most atmospheric disturbances cross the Boundary Bay region from the west and southwest (i.e., are propagating to the NE and E). Therefore, we selected four directions (210º, 240º, 270º and 300º True) and two realistic disturbance speeds (15 and 35 m/s) to compute the spatial distributions of maximum sea level wave amplitudes (Figures 13 and 14) and maximum currents speeds (Figures 15 and 16) in the study region.

The results of the eight computations reveal that the propaation direction is not a critical factor, in that the general character of the simulated wave fields and maximum wave amplitudes are similar for each scenario (Figures 13 and 14). For the disturbance speed U = 15 m/s, and for all four selected disturbance directions, the maximum computed wave amplitudes are observed on the southeast coast of the bay, close to the entrance, while on the main (northwest) coast of the bay these heights are small (Figure 13). The most effective direction is 300º True. For this direction, the maximum wave amplitudes reach 50 cm on the SE coast of the bay (Figure 13d); the least effective direction is 210º True, for which the maximum amplitudes for the entire region are < 35 cm (Figure 13a).

The differences among computed wave fields are much more significant for different disturbance speeds (Figures 13 and 14). The maximum wave amplitudes for U = 35 m/s reach more than 50-55 cm and occur on the coast of Point Roberts, the southernmost tip of the Tsawwassen Peninsula (Figure 10), and along the shelf-break at the entrance to Boundary Bay. It is clearly apparent that the shelf-break effectively reflects the incoming waves, hindering the ability of the meteotsunami to penetrate into the bay and reach the NW coast (Figure 14).

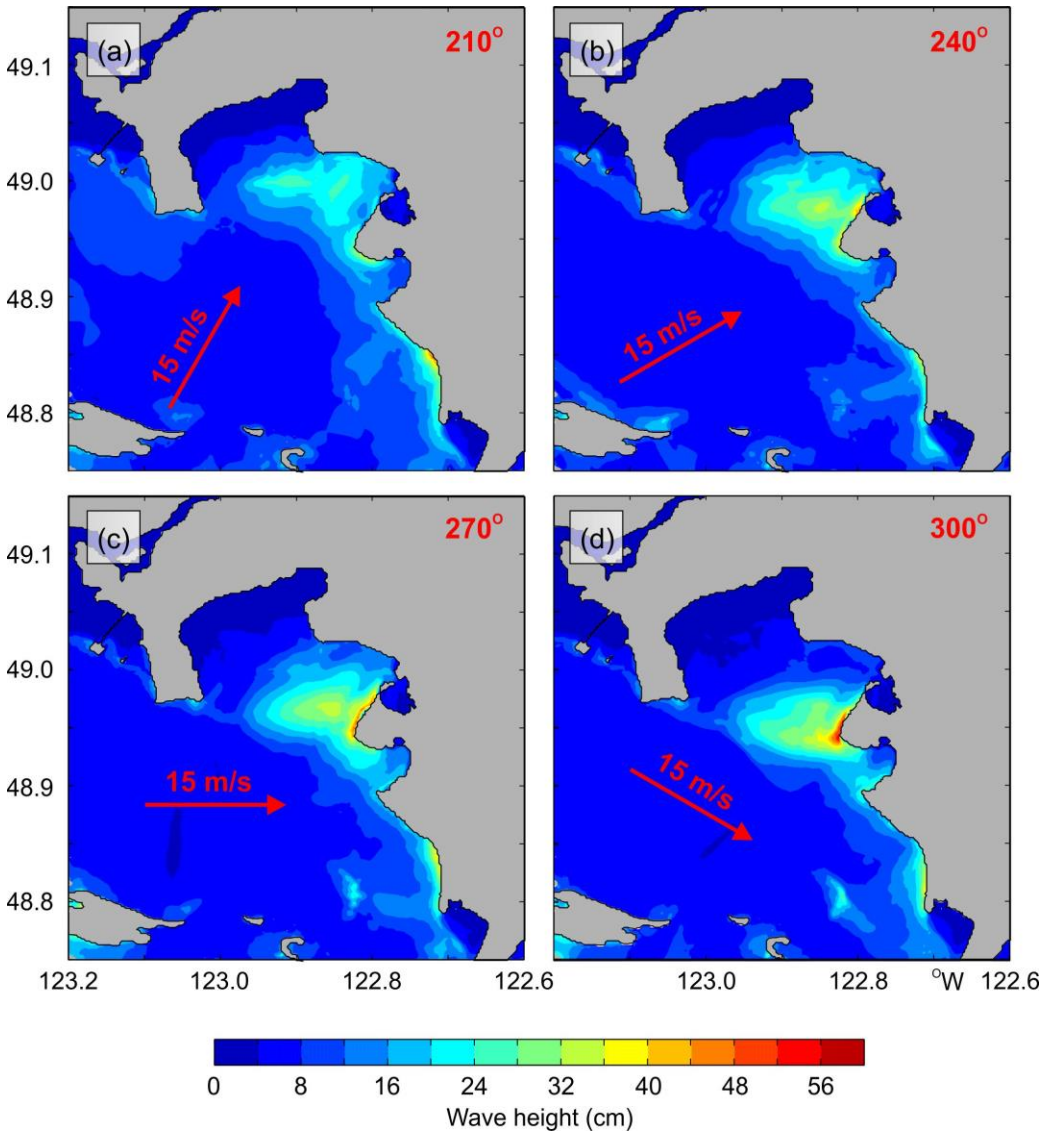

Figure 13. Maximum sea level wave amplitudes for the Boundary Bay region computed for the propagation disturbance speed of 15 m/s and four disturbance directions: 210º, 240º, 270º and 300º True.

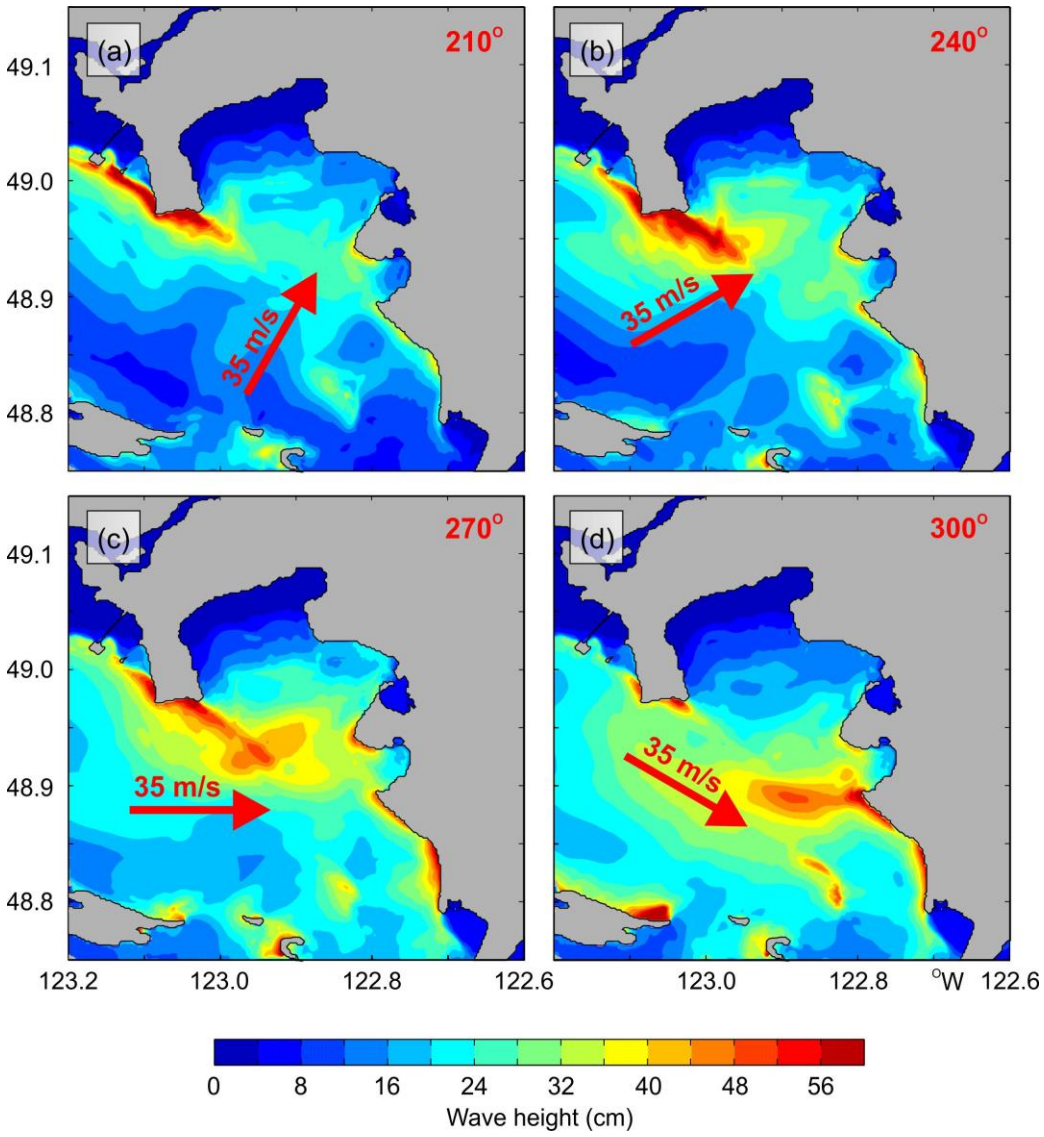

Figure 14. The same as in Figure 13 but for the propagation disturbance speed of 35 m/s.

The spatial distributions of the maximum computed current velocities (Figures 15 and 16) are in good agreement with those for the computed sea level wave amplitudes (Figures 13 and 14). For the disturbance speed U = 15 m/s, the maximum speeds (>15-20 cm/s) occur along the east coast of the bay and also along the external (southern) and internal (northern) shelf-breaks (Figure 15). No strong currents are observed in the inner part of the bay. For U = 35 m/s, the computed maximum currents are considerably stronger than for 15 m/s (Figure 16), especially for two regions: (1) the Point Roberts area and the Tsawwassen Ferry Terminal (Figure 10), and (2) the east mainland coast, where the computed current speeds reach 25 cm/s. However, even for this

disturbance speed, the inner part of Boundary Bay adjacent to the NW coast is affected by weak currents of <4 cm/s.

In general, the spatial fields of maximum computed sea level amplitudes and current speeds shown in Figures 13-16 support the conclusions presented in Sections 4.1 and 4.2, namely that the local topography of Boundary Bay and environ shelters the coast from the incoming waves, protecting the region from significant sea level oscillations and currents associated with meteotsunamis generated in the southern Strait of Georgia.

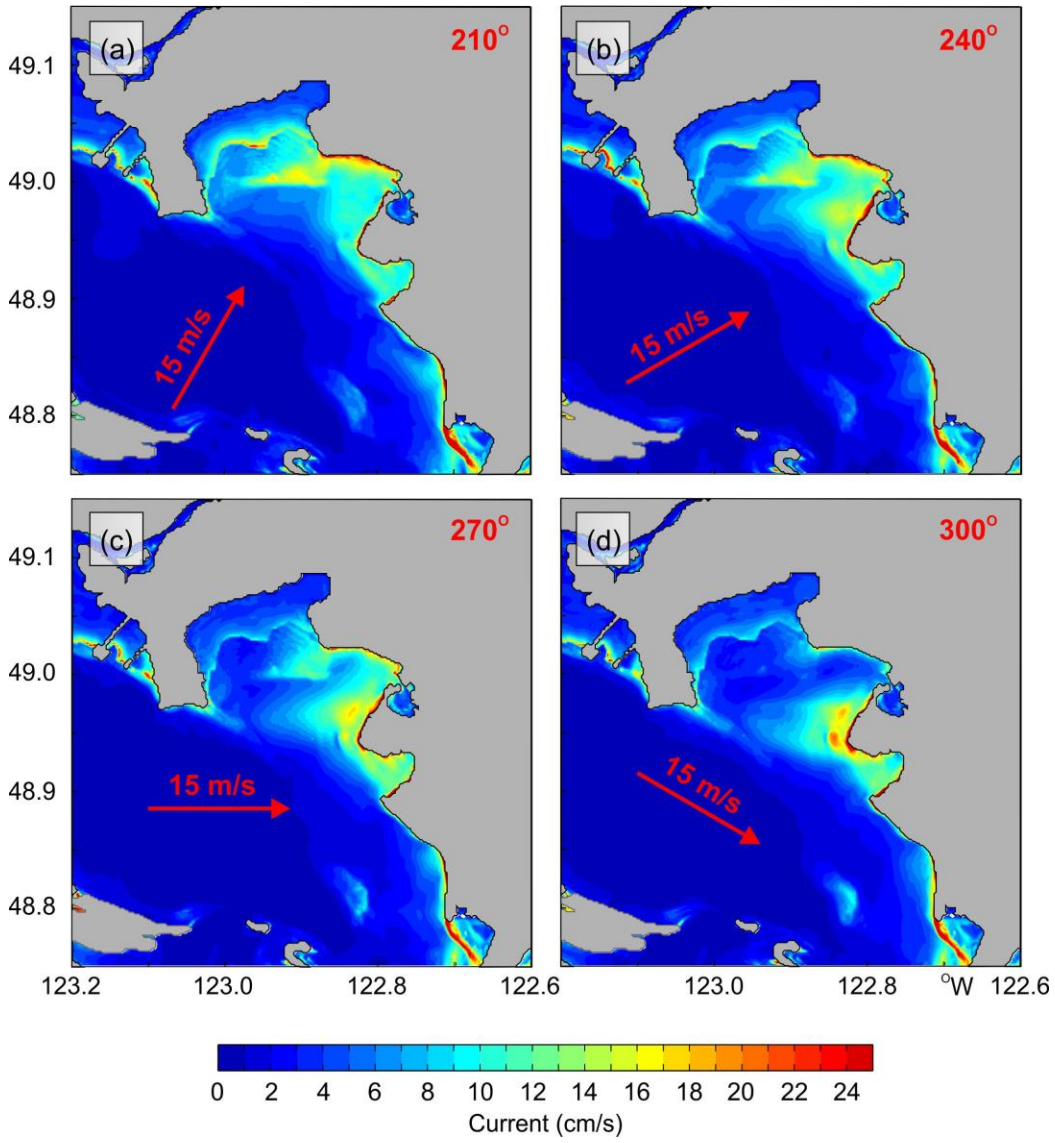

Figure 15. The same as in Figure 13 but for the maximum current speeds.

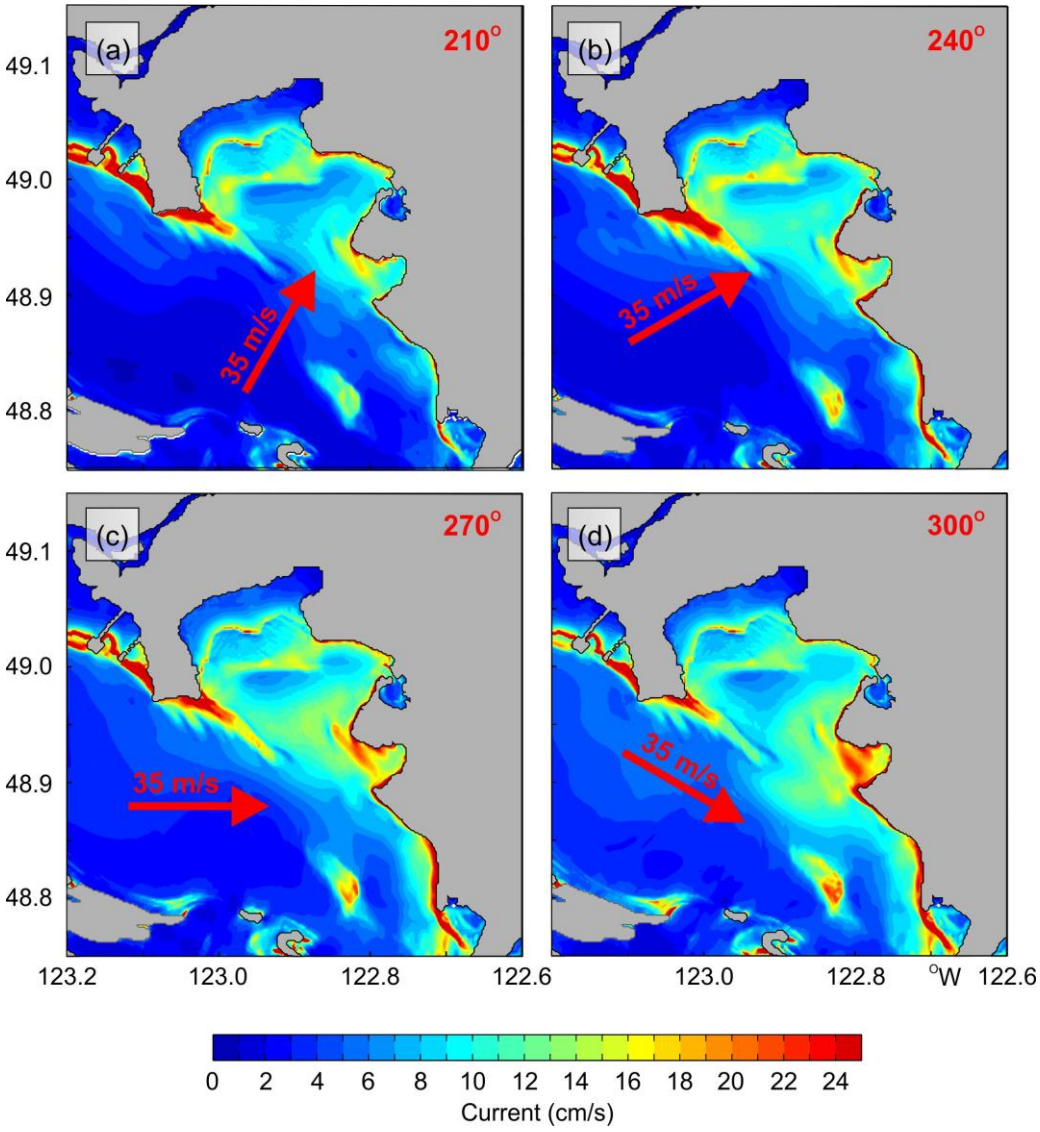

Figure 16. The same as in Figure 14 but for the maximum current speeds.

5. CONCLUSIONS

Because they have been found to be much more widespread and locally destructive than was previously thought, meteorological tsunamis have attracted considerable attention in recent years. The high meteotsunami risk for some exceptional locations ("hot spots") is mainly related to a combination of shelf topography and coastline geometry that create favourable resonant conditions

that amplify incoming waves to produce strong sea level oscillations and intense associated currents.

A number of meteotsunamis were recorded during the period 2005-2020 on the coast of British Columbia, including the southern Strait of Georgia and Juan de Fuca Strait [*Stephenson and Rabinovich*, 2009; *Thomson et al.*, 2009; *Rabinovich et al.*, 2020]. This region, including Boundary Bay, is of specific concern because of the common occurrence of significant atmospheric disturbances in the area [cf. *Thomson et al.,* 2009]. *Rabinovich et al.* [2019] focused their study on analysis of non-seismic tsunami-like waves in the southern Strait of Georgia based on examination of a 11-year (2008-2018) dataset of 1-min records from three nearby tide gauges: Point Atkinson (CHS), Cherry Point and Friday Harbor (NOAA). A statistical analysis of these records demonstrated that small but noticeable meteotsunamis (with wave heights >10 cm) occur often in this region, although no damaging events had been observed. Also, the results of this study, as well as the recent comprehensive study of some particular events [*Rabinovich et al.*, 2020], indicate a very strong influence of local topographic features on such events and high spatial variability of generated atmospherically-induced extreme sea level oscillations. For these reasons, reliable determination of the meteotsunami risk for the Boundary Bay region requires additional data inside the bay and/or high-resolution numerical modelling.

No sea level or current velocity data are presently available for Boundary Bay. Therefore, the only possibility for estimating meteotsunami impacts for the region (the purpose of the present study) is to conduct numerical modelling of sea level oscillations and currents for the southern Strait of Georgia that encompasses the Boundary Bay region. As part of that study, Section 2 briefly overviews the problem of numerical simulation of meteotsunamis, which is a much more complicated and difficult problem than modelling of seismically-induced tsunamis. Section 3, based on the study by *Rabinovich et al.* [2020], uses measured atmospheric disturbances D1-D4 to simulate the actual meteotsunami on 1 November 2010. We used the physical parameters (propagation speed and direction) derived for these four disturbances to force numerical simulations of the event and compared the results to observations from selected tide gauge sites in the strait. The numerical experiments revealed strongly individual sea level responses at each site to changing air pressure disturbance speed, direction and intensity, such that each location has its own set of "site-specific" air pressure characteristics that produce the strongest sea level response.

Differences in the local topography and coastline geometry appear to be responsible for the different responses among sites.

We consider Section 4, which uses the numerical model described in Section 3 to simulate meteotsunamis for the Boundary Bay region, to be the central part of this report. A wide range of disturbance speeds was considered, from 10 to 70 m/s, with an increment of 5 m/s, along with a full circle of propagation directions, with azimuths from 0º to 360º True at 10º increments. We found that the maximum amplitudes of generated oscillations increase shoreward, from 5-6.5 cm in the open Strait of Georgia, to 31 cm at the shelf-break, to 51 cm at the entrance to the bay. The shelf-break effectively shelters the inner part of the bay. In general, the coastal geometry and local bathymetry of Boundary Bay strongly attenuate the incoming waves, sheltering the region from significant meteotsunamis. Meteotsunami-generated currents for the Boundary Bay region are weak (maximum currents are up to 11.5 cm/s) and not a serious hazard.

We selected four directions of incoming atmospheric disturbances (210º, 240º, 270º and 300º True) and two realistic disturbance speeds, U (15 and 35 m/s), and computed the spatial distributions of the maximum sea level wave heights and maximum currents generated by these events in the study region. We found that, for U = 35 m/s, the computed maximum current velocity is considerably stronger than for U = 15 m/s, especially for the areas of Point Roberts and the Tsawwassen Ferry Terminal, and for the east mainland coast, where the computed current speeds reach 25 cm/s. However, meteotsunami-induced currents within the inner part of Boundary Bay adjacent to the northwest shore are weak (<4 cm/s). In general, the spatial fields of maximum computed sea level amplitudes and current speeds support the conclusion that the local topography of the Boundary Bay region shelters the shoreline of the bay from incoming waves, protecting this coast from significant sea level oscillations and currents associated with meteotsunamis generated in the southern Strait of Georgia.

REFERENCES

Bechle, A.J. and Wu, C.H. (2014), The Lake Michigan meteotsunamis of 1954 revisited, *Natural Hazards, 74* (1), 155-177; doi:10.1007/978-3-319-12712-5_9.

Ewing, M., Press, F., and Donn, W.L. (1954), An explanation of the Lake Michigan wave of 26 June 1954. *Science, 120*, 684-686.

Fine, I.V., Cherniawsky, J.Y., Thomson, R.E., Rabinovich, A.B., and Krassovski, M.V. (2015), Observations and numerical modeling of the 2012 Haida Gwaii tsunami off the coast of British Columbia. *Pure and Applied Geophysics, 172*(3-4), 699-718.

Fujii, Y. and Satake, K. (2007), Tsunami source of the 2004 Sumatra-Andaman earthquake inferred from tide gauge and satellite data. *Bulletin of the Seismological Society of America, 97*, S192-S207.

Heidarzadeh, M., Šepić, J., Rabinovich, A.B., Allahyar, M., Soltanpour, A., and Tavakoli, F. (2020), Meteorological tsunami of 19 March 2017 in the Persian Gulf: Observations and analyses. *Pure and Applied Geophysics, 177*(3), 1231-1259; doi: 10.1007/s00024-019-02263-8.

Kim, J. and Omira, R. (2021), The July 6-7, 2010 meteotsunami along the coast of Portugal: Insights from data analysis and numerical modeling. *Natural Hazards, 106*(2), 1397-1419; doi:10.1007/s11069-020-04335-8 .

Kowalik, Z., Knight, W., Logan, T., and Whitmore, P. (2007), The tsunami of 26 December, 2004: Numerical modeling and energy considerations. *Pure and Applied Geophysics, 164*(2-3), 379-393.

Kowalik, Z. (2012), *Introduction to Numerical Modeling of Tsunami Waves*, Institute of Marine Science, University of Alaska, Fairbanks. 195 pp. https://www.sfos.uaf.edu/directory/faculty/kowalik/Tsunami_Book/book_sum.pdf

Monserrat, S. and Thorpe, A.J. (1992), Gravity-wave observations using an array of microbarographs in the Balearic Islands, *Quarterly Journal of the Royal Meteorological Society, 118*, 259-282.

Monserrat, S., Rabinovich, A.B., and Casas, B. (1998), On the reconstruction of the transfer function for atmospherically generated seiches. *Geophysical Research Letters, 25*(12), 2197-2200.

Monserrat, S., Vilibić, I., and Rabinovich, A.B. (2006), Meteotsunamis: Atmospherically induced destructive ocean waves in the tsunami frequency band, *Natural Hazards and Earth System Sciences*, 6, 1035-1051.

Monserrat, S., Fine, I., Amores, A., and Marcos, M. (2014), Tidal influence on high frequency harbor oscillations in a narrow entrance bay, *Natural Hazards*, *74*, 143-153; doi:10.1007/s11069-014-1284-3.

Orlić, M., Belušić, D., Janeković, I., and Pasarić, M. (2010), Fresh evidence relating the great Adriatic surge of 21 June 1978 to mesoscale atmospheric forcing, *Journal of Geophysical Research - Oceans*, *115*, C06011, doi:10.1029/2009JC005777.

Pattiaratchi, C.B. and Wijeratne, E.M.S. (2015), Are meteotsunamis an underrated hazard? *Philosophical Transactions of the Royal Society*, *A* 373, 20140377, 1-23.

Proudman, J. (1929), The effects on the sea of changes in atmospheric pressure, *Geophysical Supplement, Monthly Notices of the Royal Astronomical Society*, 2, 197-209.

Rabinovich, A.B. (2009), Seiches and harbor oscillations, in *Handbook of Coastal and Ocean Engineering* (edited by Y.C. Kim), Chapter 9, World Scientific Publ., Singapore, 193-236.

Rabinovich, A.B. (2020), Twenty-seven years of progress in the science of meteorological tsunamis following the 1992 Daytona Beach event, *Pure and Applied Geophysics*, *177*(3),1193-1230; doi: 10.1007/s00024-019-02349-3.

Rabinovich, A.B. and Monserrat, S. (1996), Meteorological tsunamis near the Balearic and Kuril Islands: Descriptive and statistical analysis. *Natural Hazards*, *13*, 55-90.

Rabinovich, A.B., Monserrat, S., and Fine, I.V. (1999), Numerical modeling of extreme seiche oscillations in vicinity of the Balearic Islands. *Okeanology*, *39*(1), 16-24.

Rabinovich, A.B., Thomson, R.E., Bornhold, B.D., Fine, I.V., and Kulikov, E.A. (2003), Numerical modelling of tsunamis generated by hypothetical landslides in the Strait of Georgia, British Columbia. *Pure and Applied Geophysics*, *160*(7), 1273-1313.

Rabinovich, A.B., Candella, R.N., and Thomson, R.E. (2011), Energy decay of the 2004 Sumatra tsunami in the World Ocean. *Pure and Applied Geophysics*, *168*(11), 1919-1950.

Rabinovich, A.B., Titov, V.V., Moore, C.W., and Eblé, M.C. (2017), The 2004 Sumatra tsunami in the Southern Pacific Ocean: new global insight from observations and modeling. *Journal of Geophysical Research-Ocean*, *122*(10), 7992-8019.

Rabinovich, A.B., Šepić, J., and Thomson, R.E. (2019), Meteorological tsunamis on the south coast of British Columbia with application to Boundary Bay, Canadian Technical Report of Hydrography and Ocean Sciences, Fisheries and Oceans Canada, Institute of Ocean Sciences, Sidney.

Rabinovich, A.B., Šepić, J., and Thomson, R.E. (2021), The meteorological tsunami of 1 November 2010 in the southern Strait of Georgia: A case study, *Natural Hazard, 106*(2), 1503-1544; doi: 10.1007/s11069-020-04203-5.

Rabinovich, A.B., Šepić, J., and Thomson, R.E. (2023), Strength in numbers: The tail end of typhoon Songda combines with local cyclones to generate extreme sea level oscillations on the British Columbia and Washington Coasts during Mid-October 2016, *Journal of Physical Oceanography, 53*(1), 131-155; doi:10.1175/JPO-D-22-0096.1.

Salaree, A., Mansouri, R., and Okal, E.A. (2018), The intriguing tsunami of 19 March 2017 at Bandar Dayyer, Iran: Field survey and simulations, *Natural Hazards, 90*(3), 1277–1307.

Šepić, J. and Rabinovich, A.B. (2014), Meteotsunamis in the Great Lakes and on the Atlantic coast of the United States generated by the "derecho" of 29-30 June 2012. *Natural Hazards, 74*, 75-108, doi: 10.1007/s11069-014-1310-5.

Šepić, J., Vilibić, I., Rabinovich, A.B., and Monserrat, S. (2015), Widespread tsunami-like waves of 23-27 June in the Mediterranean and Black Seas generated by high-altitude atmospheric forcing, *Scientific Reports, 5*(11682), 1-5; doi:10.1038/srep11682.

Šepić, J., Međugorac, I., Janeković, I., Dunić, N., and Vilibić, I. (2016), Multi-meteotsunami event in the Adriatic Sea generated by atmospheric disturbances of 25–26 June 2014. *Pure and Applied Geophysics*, *173*(12), 4117-4138; doi: 10.1007/s00024-016-1249-4.

Šepić, J., Rabinovich, A.B., and Sytov, V.N. (2018), Odessa tsunami of 27 June 2014: Observations and numerical modelling. *Pure and Applied Geophysics, 175*(4), 1545-1572.

Stephenson, F.E., and Rabinovich, A.B. (2009), Tsunamis on the Pacific coast of Canada recorded in 1994-2007. *Pure and Applied Geophysics, 166*(1-2), 177-210.

Thomson, R.E., Rabinovich, A.B., Fine IV et al. (2009), Meteorological tsunamis on the coasts of the British Columbia and Washington. *Physics and Chemistry of the Earth, 34*, 971-988.

Titov, V.V. and González, F.I. (1997), Implementation and testing of the Method of Splitting Tsunami (MOST) model. *Technical Report NOAA Tech. Memo. ERL PMEL-112* (PB98-122773), NOAA/Pacific Marine Environmental Laboratory Seattle, WA.

Titov, V.V. and Synolakis, C.E. (1998), Numerical modeling of tidal wave runup. *Journal of Waterway Port Coastal and Ocean Engineering-ASCE, 124*(4), 157-171.

Titov, V., Rabinovich, A.B., Mofjeld, H.O., Thomson, R.E., and González, F.I. (2005), The global reach of the 26 December 2004 Sumatra tsunami. *Science, 309*(5743), 2045-2048.

Titov, V., Song, Y.T., Tang, L., Bernard, E.N., Bar-Sever, Y., and Wei, Y. (2016), Consistent estimates of tsunami energy show promise for improved early warning. *Pure and Applied Geophysics, 173*(12), 3863-3880.

Titov, V. and Moore, C. (2020), Meteotsunami model forecast: Can coastal hazard be quantified in real-time? *Natural Hazards, 106*(2), 1545-1561; doi:10.1007/s11069-020-04450-6.

Vilibić, I., Domijan, N., Orlić, M., Leder, N., and Pasarić, M. (2004), Resonant coupling of a traveling air pressure disturbance with the east Adriatic coastal waters, *Journal of Geophysical Research - Oceans, 109*, C10001, doi:10.1029/2004JC002279.

Vilibić, I., Monserrat, S., Rabinovich, A.B., and Mihanović, H. (2008), Numerical modelling of the destructive meteotsunami of 15 June 2006 on the coast of the Balearic Islands. *Pure and Applied Geophysics, 165*, 2169-2195.

Vilibić, I., Šepić, J., Ranguelov, B., Strelec Mahović, N., and Tinti, S. (2010). Possible atmospheric origin of the 7 May 2007 western Black Sea shelf tsunami event. *Journal of Geophysical Research-Oceans, 115*, C07006; doi: 10.1029/2009JC005904.

Weaver AJ, Wiebe EC (2006) Micrometeorological network in Greater Victoria schools: www.victoriaweather.ca. *CMOS Bulletin, 34*(4):184-190.